Global Change Biology
celebrating 20 years

Global Change Biology (2014) **20**, 1191–1210, doi: 10.1111/gcb.12443

A high-resolution approach to estimating ecosystem respiration at continental scales using operational satellite data

JONAS JÄGERMEYR*†, DIETER GERTEN*, WOLFGANG LUCHT*†, PATRICK HOSTERT†, MIRCO MIGLIAVACCA‡§ and RAMAKRISHNA NEMANI¶

*Potsdam Institute for Climate Impact Research, RD 1: Earth System Analysis, PO-Box 601203, D-14412 Potsdam, Germany, †Geography Department, Humboldt-Universität zu Berlin, Unter den Linden 6, D-10099 Berlin, Germany, ‡Max Planck Institute for Biogeochemistry, Department Biogeochemical Integration, Hans-Knöll-Str. 10, D-07745, Jena, Germany, §Remote Sensing of Environmental Dynamics Laboratory, DISAT, Università degli Studi Milano-Bicocca, Piazza della Scienza, 1, 20126 Milan, Italy, ¶NASA Ames Research Center, Moffett Field, CA 94035, USA

Abstract

A better understanding of the local variability in land-atmosphere carbon fluxes is crucial to improving the accuracy of global carbon budgets. Operational satellite data backed by ground measurements at Fluxnet sites proved valuable in monitoring local variability of gross primary production at highly resolved spatio-temporal resolutions. Yet, we lack similar operational estimates of ecosystem respiration (Re) to calculate net carbon fluxes. If successful, carbon fluxes from such a remote sensing approach would form an independent and sought after measure to complement widely used dynamic global vegetation models (DGVMs).

Here, we establish an operational semi-empirical Re model, based only on data from the Moderate Resolution Imaging Spectroradiometer (MODIS) with a resolution of 1 km and 8 days. Fluxnet measurements between 2000 and 2009 from 100 sites across North America and Europe are used for parameterization and validation.

Our analysis shows that Re is closely tied to temperature and plant productivity. By separating temporal and inter-site variation, we find that MODIS land surface temperature (LST) and enhanced vegetation index (EVI) are sufficient to explain observed Re across most major biomes with a negligible bias [R^2 = 0.62, RMSE = 1.32 (g C m^{-2} d^{-1}), MBE = 0.05 (g C m^{-2} d^{-1})].

A comparison of such satellite-derived Re with those simulated by the DGVM LPJmL reveals similar spatial patterns. However, LPJmL shows higher temperature sensitivities and consistently simulates higher Re values, in high-latitude and subtropical regions. These differences remain difficult to explain and they are likely associated either with LPJmL parameterization or with systematic errors in the Fluxnet sampling technique. While uncertainties remain with Re estimates, the model formulated in this study provides an operational, cross-validated and unbiased approach to scale Fluxnet Re to the continental scale and advances knowledge of spatio-temporal Re variability.

Keywords: FLUXNET, land surface temperature, LPJmL DGVM, MODIS, RECO, temperature sensitivity, terrestrial carbon flux, up-scaling

Received 22 March 2013 and accepted 9 October 2013

Introduction

Global terrestrial Gross Primary Production (GPP) and Ecosystem Respiration (Re) are roughly estimated to be 123 Pg C a^{-1} (Beer *et al.*, 2010), and 103 Pg C a^{-1} (Yuan *et al.*, 2011), respectively. Small changes in these large fluxes can have significant impact on atmospheric CO_2 concentrations on an interannual time-scale. Terrestrial carbon pools and flux rates, however, are insufficiently understood and remain associated with large uncertainties (Schimel *et al.*, 2001; Sabine *et al.*, 2004; Beer *et al.*, 2010; Jung *et al.*, 2011). The terrestrial land sink, that is, the marginal remainder of GPP and Re, has been highly variable over the last three decades (Denman *et al.*, 2007; Le Quéré *et al.*, 2009; Pan *et al.*, 2011) and its future resilience is uncertain (e.g., Cramer *et al.*, 2001; Canadell *et al.*, 2007; Heimann & Reichstein, 2008; Bond-Lamberty & Thomson, 2010). It is particularly Re that is difficult to constrain at the global scale due to limited understanding of complex interactions of physical, chemical, and biological processes and resulting high spatio-temporal dynamics.

Dynamic Global Vegetation Models (DGVMs) simulate land-atmosphere carbon fluxes on the global scale based on mechanistic dependencies (e.g., Sitch *et al.*, 2003; Krinner, 2005), but they are limited by our understanding of processes and their appropriate

Correspondence: J. Jägermeyr, tel. +49 331 288 2656, fax +49 331 288 2620, e-mail: jonas.jaegermeyr@pik-potsdam.de

parameterization and by coarse resolution input data (e.g., climate and soil structure). Re estimates from DGVMs critically rely on the implemented temperature sensitivity (Jones *et al.*, 2003), which is subject to ongoing discussion and it has recently been challenged to be overestimated (Mahecha *et al.*, 2010). The temperature sensitivity is a directly important parameter in the analysis of climate change impacts on global respiratory processes and on high-latitude soil carbon stocks in particular. Several biotic and abiotic factors limit the response to temperature, but their interactions (Davidson *et al.*, 2006a; Kirschbaum, 2006) and time-scale dependency are still under discussion (Kirschbaum, 2010; Yvon-Durocher *et al.*, 2012). While DGVMs form our primary measure to simulate future responses of carbon pools to altered environmental conditions, their limitations distract from enhancing our understanding of unconstrained spatio-temporal dynamics of current Re patterns.

Operational and reliable remote sensing products with weekly 1 km resolution backed by Fluxnet data form a new important measure for empirically up-scaling small-scale ground measurements to the global scale. The Fluxnet program (ORNL, 2011) provides a global network of standardized quasi-continuous eddy covariance carbon flux measurements for over a decade (Aubinet *et al.*, 2000; Baldocchi *et al.*, 2001; Papale, 2006). Tower distribution is too sparse to adequately represent global ecological heterogeneity, but the database allows to draw powerful empirical relations to predict Re across biomes. Current remote sensing products, such as from the Moderate Resolution Imaging Spectroradiometer (MODIS), provide key ecosystem variables at unmatched spatial and temporal resolutions, which allow up-scaling of locally trained parameters to the continental-scale (Mahadevan *et al.*, 2008; Jung *et al.*, 2009, 2011; Xiao *et al.*, 2011, 2012).

This data-driven approach is capable of tracking spatio-temporal variability with high resolution and is therefore suitable to reduce uncertainties associated to current estimates of the global carbon cycle and further to complement and challenge theory-based DGVM estimates. Comparing such inherently different approaches is an important step to arrive at a more conclusive picture. If DGVM simulations proof instrumental to simulating convincingly observed patterns, confidence in future projections could be increased (Friedlingstein *et al.*, 2006; Heimann & Reichstein, 2008).

The validity of simple, semi-empirical models for predicting Fluxnet Re at the plot scale has been shown (Richardson *et al.*, 2006a; Reichstein *et al.*, 2007; Migliavacca *et al.*, 2011). Further, readily available MODIS products show strong correlations with those dependencies (e.g., Rahman *et al.*, 2005; Huang & Niu, 2013), but the large-scale link-up of both has not yet been fully exploited. While GPP is estimated with reasonable success at the global scale with 1 km and 8 day MODIS data (Running *et al.*, 2004; Heinsch & Zhao, 2006; Yang *et al.*, 2007; Sims *et al.*, 2008), Re remains less constrained, because it has been difficult to explain a sufficient degree of spatial, that is, intersite variability across biomes. Re has been often linked to temperature only, without accounting for plant productivity or soil moisture limitations (Yamaji *et al.*, 2007; Olofsson *et al.*, 2008; Schubert *et al.*, 2010). Other studies advanced Re estimates by the additional account for plant productivity through vegetation indicies (Vourlitis *et al.*, 2003; Gilmanov *et al.*, 2005; Loranty *et al.*, 2010). Further, Kimball *et al.* (2009) estimated net carbon fluxes with a multi-pool carbon model using satellite microwave temperature and moisture data. However, all studies above remain restricted to mid- to high latitude regions. The potential of MODIS Land Surface Temperature (LST) and Enhanced Vegetation Index (EVI) to directly estimate per-pixel Re across biomes was highlighted by Rahman *et al.* (2005) and Sims *et al.* (2008), but they never presented a corresponding model. Following a different approach, Jung *et al.* (2011) trained a model tree ensemble to operationally predict GPP and Re at the global scale. This greatly advances estimating global numbers by Fluxnet up-scaling, but its 0.5° and monthly resolution is not sufficient to monitor local spatio-temporal variability and it is also not truly remote sensing based, involving *in situ* measured and modeled meteorological data. Independent cross-biome continental-scale remote sensing Re estimates at the 1 km and 8 day resolution have not reached operational basis.

In this study, we developed a data-driven, yet physiologically meaningful remote sensing-based model for broad-scale operational estimates of Re, hereafter referred to as RECO. Two reasons render its urgency: (i) it lacks Re for combining it with existing GPP estimates from previous studies (e.g., Sims *et al.*, 2008) to calculate per-pixel Net Ecosystem Exchange (NEE) at the resolution of 1 km and 8 days. This would directly contribute to reducing uncertainties associated with local dynamics of the global carbon cycle. (ii) it is of great value to develop a data-driven and thus independent measure to complement theory-based DGVM estimates. RECO is driven by MODIS Land Surface Temperature (LST) and Enhanced Vegetation Index (EVI) with the typical MODIS resolution of 1 km and 8 days. Water stress is accounted for through difference between day- and nighttime LST and plant activity through EVI. Fluxnet data from 100 sites across major biomes in North America and Europe build the reference for training and validation. Since validation of continental-scale Re is not feasible, we compare our result

with continental-scale patterns of Re from an independent process-based DGVM, namely the Lund-Potsdam-Jena managed Land model (Sitch *et al.*, 2003; Schaphoff *et al.*, 2013). LPJmL is a well-known and validated DGVM suited to simulate Re from natural and managed land covers, based on climate and soil input only. The comparison is conducted in a bidirectional way: We test if RECO is able to reproduce simulated large-scale patterns from LPJmL and thus if such an up-scaling approach can be considered representative for the investigated biomes. On the other hand, we test to what degree such independent approaches agree and where regions of uncertainty are located. Further, we compare empirically fitted temperature sensitivities in RECO with those implemented in LPJmL to study the contribution of these parameterizations to model differences.

Materials and methods

Model development

Ecosystem respiration consists of Autotrophic Respiration (Ra), which is the growth and maintenance respiration of leaves, stems, and roots, and Heterotrophic Respiration (Rh), which accounts for belowground decomposition by the microbes and soil fauna (e.g., Raich & Tufekciogul, 2000; Ryan & Law, 2005),

$$\mathrm{Re} = \mathrm{Ra} + \mathrm{Rh}. \quad (1)$$

NEE is defined as the difference between Re and GPP:

$$\mathrm{NEE} = \mathrm{Re} - \mathrm{GPP}. \quad (2)$$

It is not feasible to disentangle the complex interactions of surface and subsurface processes contributing to Re by means of remote sensing. Yet, on the time-scale of days, simplified empirical approaches have proven instrumental to estimating Re in its seasonality and magnitude (Richardson *et al.*, 2006a; Reichstein & Beer, 2008; Migliavacca *et al.*, 2011). Our modeling strategy is based on the following assumptions. Temperature (Lloyd & Taylor, 1994; Raich & Tufekciogul, 2000) and plant productivity (Janssens *et al.*, 2001; Kuzyakov & Gavrichkova, 2010) are the predominant drivers of short-term temporal variation, which can be limited by water stress (Raich & Schlesinger, 1992; Reichstein *et al.*, 2007). We link variation in magnitude of Re between sites and years (interyear differences, e.g., due to disturbances and management) to mean annual plant productivity (Janssens *et al.*, 2001; Yuan *et al.*, 2011) and to mean annual temperature (Raich & Schlesinger, 1992; Bond-Lamberty & Thomson, 2010). Furthermore, we assume that plant productivity can explain short-term variations in Re as well as long-term and spatial differences, because GPP is directly linked to Ra and because organic matter sustains above- and belowground decomposition through litter fall (e.g., Bahn *et al.*, 2010). We link each of these semi-empirical dependencies to operational remote sensing products below.

Parameters are estimated for six aggregated functional biomes, which are based on Koeppen-Geiger climate classification (Peel *et al.*, 2007; ORNL, 2010) and the International Geosphere-Biosphere Program (IGBP) classification scheme from the MODIS land cover product (Friedl *et al.*, 2002). We stratify climate classes based on their temperature and precipitation regime into three climate types: (i) Temperature-Limited (TL, cold and polar climates), (ii) Temperate and Humid (TH, temperate, not summer dry) and (iii) Water-Limited (WL, semi-arid with summer dry period). Further, we divide each climate type into two functional aggregated land cover types: (i) forests (FOR) and (ii) non-forested natural vegetation or croplands (GRA/CRO). Only vegetated areas are investigated. Figure 1 displays the global distribution of aggregated biomes.

To account for spatial and seasonal variability separately, we partition Re observations into the site-specific reference respiration rate ($\mathrm{Re}_{\mathrm{ref}}$) and the remaining standardized respiration rate ($\mathrm{Re}_{\mathrm{std}}$), which is the seasonal variation, detrended for site characteristics and thus predictor responses are smoothed across sites (Fig. 2).

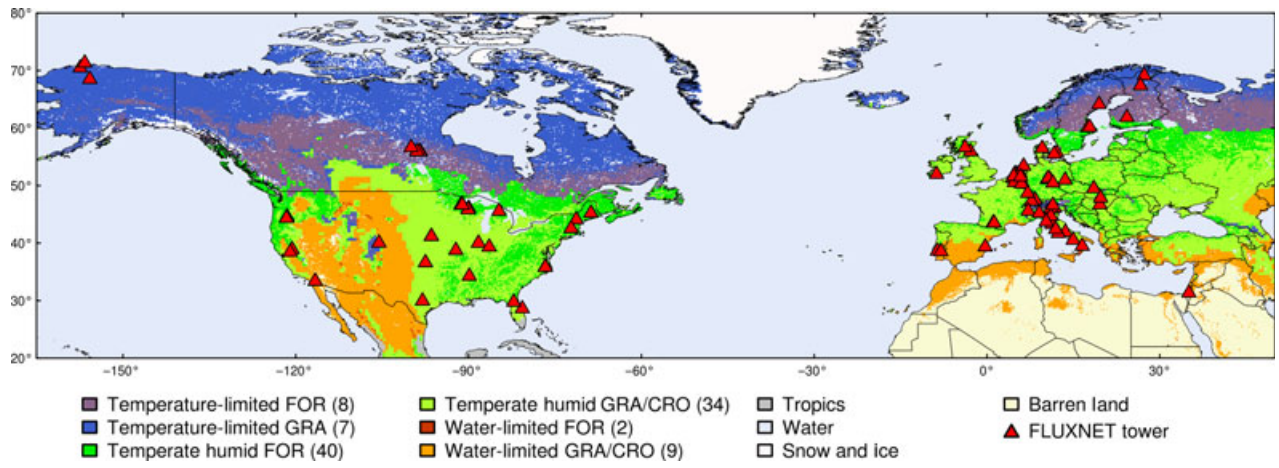

Fig. 1 Spatial distribution of aggregated biomes for which RECO is parameterized individually (FOR: forested land covers, GRA/CRO: non-forested land covers). Investigated Fluxnet sites are indicated by red triangles, numbers in brackets give the number of available sites per biome.

$$\mathrm{Re}_{[Climate,\ land\ cover]} = \mathrm{Re}_{ref} * \mathrm{Re}_{std} \quad (3)$$

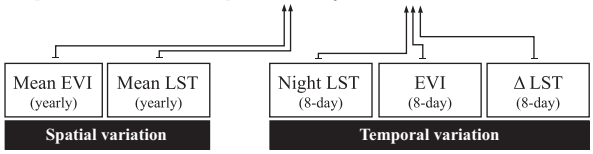

Fig. 2 Equation 3 associated with input factors contributing to Re estimates. Re_{ref} is the reference respiration rate at its reference temperature, Re_{std} is the standardized respiration rate.

Reference Respiration Rate (Re_{ref}). Re_{ref} is the respiration rate at the temperature T_{ref} (°C), which describes differences in magnitude between sites and years. T_{ref} is set to the approximate mean springtime temperature (Day of Year 96-144) for each climate type: T_{ref_TL} = 0 °C, T_{ref_TH} = 12 °C and T_{ref_WL} = 13 °C. We find that Re_{ref} becomes less suitable to capture site characteristics at higher T_{ref} values. Particularly among WL, sites water-stress confounds the temperature signal above 13 °C. Re_{ref} is extrapolated at T_{ref} through a polynomial surface from the reference data for each site and year.

In RECO, Re_{ref} is estimated as follows:

$$Re_{\mathrm{ref}} = p_1 + p_2 * EVI_{\mathrm{mean}} + p_3 * LST_{\mathrm{mean}}, \quad (4)$$

where EVI_{mean} is mean annual springtime EVI (observations within $T_{ref} \pm 3$ °C, as nighttime LST equivalent, and from first half-year), LST_{mean} is mean annual daytime LST (LST_d) and $p_{1\text{-}3}$ are free parameters. For climate types TL and WL, Re_{ref} parameterization is not further split into land cover classes FOR and GRA/CRO, because data availability is limiting. Figure 3 displays Re_{ref} dependencies to EVI_{mean} and LST_{mean}.

Standardized Respiration Rate (Re_{std}). Re_{std} is the ratio of Re and Re_{ref}. For all fitted biomes that are not water-limited (TL-FOR, TL-GRA/CRO, TH-FOR and TH-GRA/CRO), Re_{std} is estimated as follows:

$$Re_{\mathrm{std}} = \frac{p_4}{p_5 + p_6^{-\frac{LST_n - 10}{10}}} + p_7 * EVI + p_8, \quad (5)$$

where LST_n is nighttime LST (°C) and EVI refers to standardized EVI (8-day EVI divided by EVI_{mean}) and $p_{4\text{-}8}$ are free parameters. We estimate Re_{std} in case of snow cover from a separate LST_n only fit (Fig. 4).

Water stress shows a considerable impact at WL sites, which we directly account for through the difference between daytime and nighttime LST (LST_{dif}) (Cai *et al.*, 2007). This approach exploits radiation properties of changing surface soil moisture content (Schmugge, 1978; Verstraeten *et al.*, 2006; Wang & Qu, 2009). Further, we also account for water stress indirectly through EVI (e.g., Gu *et al.*, 2007; Schnur *et al.*, 2010). During periods of water limitation the temperature dependence of Re_{std} is no longer valid. Therefore, we calculate Re_{std} for the WL biome during the dry period as follows:

$$Re_{\mathrm{std}} = p_9 * EVI + p_{10} * LST_{\mathrm{dif}} + p_{11} \quad (6)$$

The remaining season in WL climates is estimated as follows:

$$Re_{\mathrm{std}} = p_{9.1} * EVI + p_{10.1} * LST_n + p_{11.1} \quad (7)$$

We define the dry season to occur between Day of Year (DoY) 136 and 272 as an empirical finding in the data. These dates delimit the summer cutback of the mean seasonal course across WL data (Fig. S2).

Fluxnet data and parameter estimation

RECO parameter estimation is based on data from the Fluxnet program between 2000 and 2009 (ORNL, 2011). We employ air temperature (Ta) and Re, which is provided as a temperature interpolation from nighttime net carbon fluxes

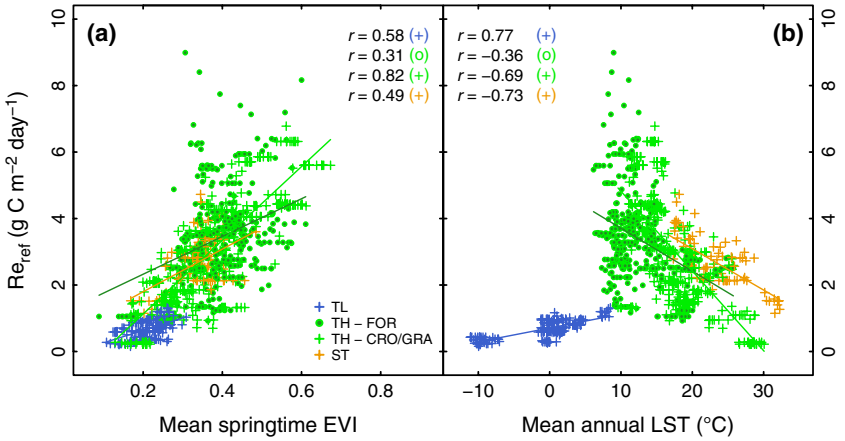

Fig. 3 Re_{ref} responses to mean springtime EVI (a) and mean LST (b), for each climate type. The Temperate Humid (TH) biome is further split into forested and non-forested sites, while Temperature-Limited (TL) and Water-Limited (WL) could not be further separated significantly. 'r' relates to Pearson's correlation coefficient. Note that Re_{ref} values are not comparable across climate classes, due to different levels of the reference temperature (T_{ref}).

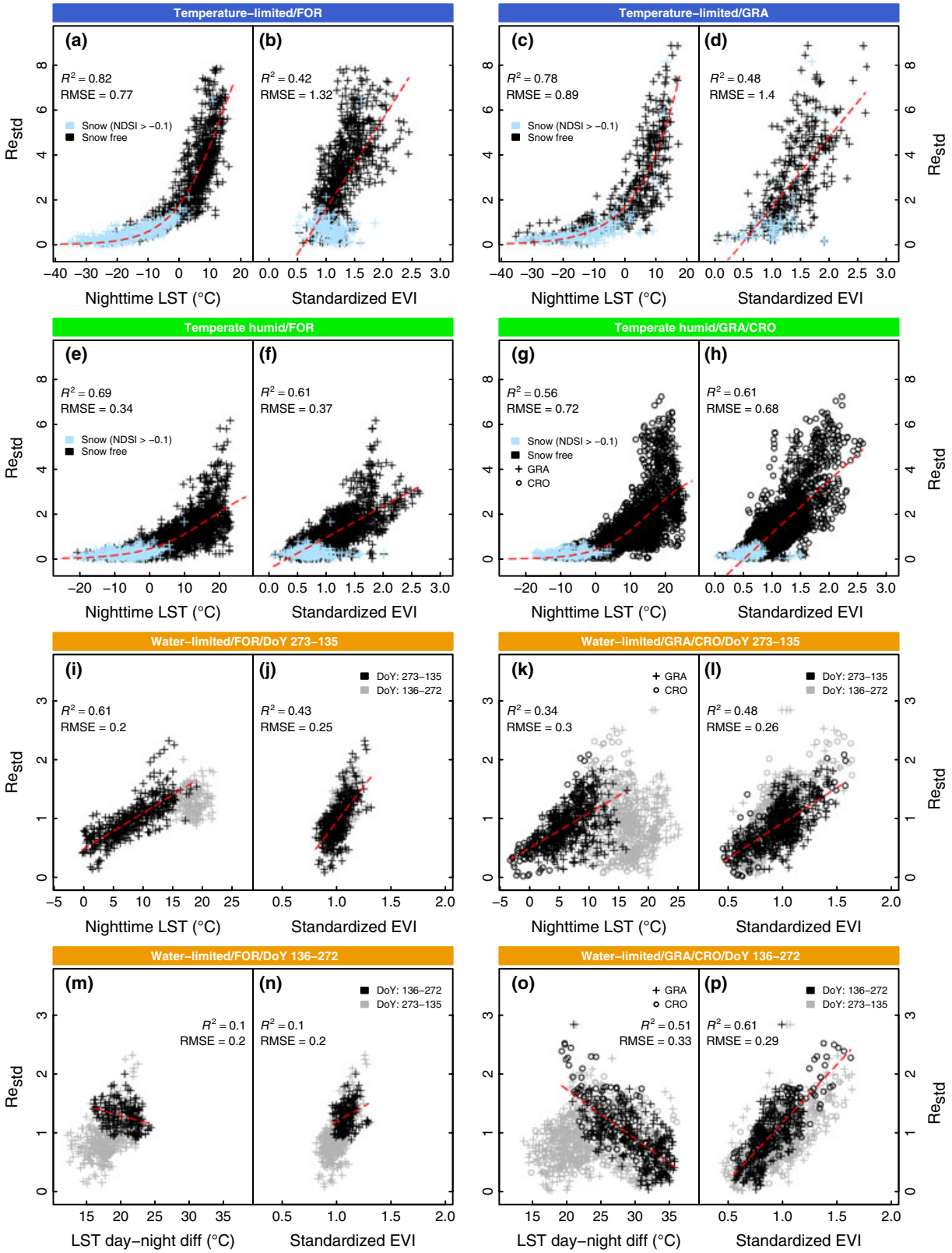

Fig. 4 Re_{std} responses to LST_n and standardized EVI (which is EVI/EVI_{mean}) for TL and TH biomes and for FOR and GRA/CRO land covers, respectively (a–h). Re_{std} responses to LSTn, LST_{dif} and standardized EVI for the WL biome stratified into non-dry season and dry season (DoY 136-272) for FOR and GRA/CRO land covers, respectively (i–p). Fitted function curves are drawn in red.

(Reichstein *et al.*, 2005). We utilize gap-filled and quality-assessed 8-day average data (Level 4, well mixed conditions) (Papale & Valentini, 2003) and we filter data by quality flag (qc > 0.9). A threefold gliding window filter is applied to smooth Re observations. To account for footprint heterogeneity we only incorporate sites which are situated within four pixels of the same 500 m aggregated MODIS land cover type (FOR or GRA/CRO). Overall, 100 sites meet our demands of data quality and footprint homogeneity and are distributed between 28.61° and 71.32°N and between −157.41° and 35.05°E (Fig. 1). Although sites are not equally distributed across biomes, and only situated in the northern hemisphere, most major non-tropical biomes are represented.

Parameters are estimated by nonlinearly minimizing the sum of squared residuals, weighted by its uncertainty (Lasslop *et al.*, 2008). LST_n and EVI show generally high level of multicollinearity; we allow values up to 0.8. A fivefold cross-validation procedure is employed to estimate and validate the parameter set. For each cycle, 80 percent of the available sites are used for model calibration and 20 percent are detained for validation. Each site is used for validation exactly once, and parameters are never evaluated against calibration sites. Continental-scale RECO application is based on parameters retrieved from the entire site data to assure most robust parameters (Table S3, S4).

The following evaluation criteria are employed: (i) correlation coefficients (r) calculated using the Pearson method, (ii) Coefficient of determination (R^2), (iii) root mean square error (RMSE), (iv) mean biased error, MBE = sum(observed-predicted)/n, (v) Estimation Uncertainty (OEU), the mean absolute error divided by mean prediction, and (vi) Akaike's Information Criterion (AIC), which is used for equation performance comparison.

MODIS data

MODIS LST is retrieved from seven Thermal Infrared (TIR) bands (Wan & Dozier, 1996). We employ the 1 km MOD11A2 and MYD11A2 V5 LST products, which are 8-day average values of cloud free observations featuring day- and nighttime estimates, respectively. We omit observations if the qc flag indicates 'bad raw data quality' or if 'average LST error' > 1 K (Wan & Li, 2008; Coll *et al.*, 2009).

We use the atmospherically corrected MOD09A1 V5 8-day surface reflectance (best observation in 8 days) at 500 m resolution to calculate EVI as follows:

$$EVI = \frac{G * (\rho_{\mathrm{NIR}} - \rho_{\mathrm{red}})}{(\rho_{\mathrm{NIR}} + C_1 * \rho_{\mathrm{red}} - C_2 * \rho_{\mathrm{blue}} + L)}, \quad (8)$$

where G is a gain factor, ρ is surface reflectance at the Near Infrared (NIR), red and blue band, L is the canopy background adjustment, and C1, C2 are coefficients of the aerosol resistance term. We adopt coefficient values from the MODIS EVI algorithm, L = 1, C1 = 6, C2 = 7.5, and G = 2.5. EVI over snow is ill-defined; therefore, we mask EVI if Normalized Difference Snow Index (NDSI) exceeds −0.1 (Salomonson & Appel, 2004). NDSI is calculated as follows:

$$NDSI = \frac{(\rho_{\mathrm{green}} - \rho_{\mathrm{SWIR}})}{(\rho_{\mathrm{green}} + \rho_{\mathrm{SWIR}})}, \quad (9)$$

where ρ is the reflectance in the green and in the Short Wave Infrared band.

Land cover is assessed using the yearly IGBP MCD12Q1 V5 500 m product. Data from 2001 to 2005 are available to this study, filtered with the quality assessment flag (confidence > 50%) and averaged across years to one static map. *In situ* land cover information is not considered, because it does not necessarily account for the entire pixel footprint.

All 8-day MODIS products are averaged over pixels indicating the same aggregated land cover class within a 3 × 3 km subset. Primarily, we use Terra products, but we also use Aqua data for gap-filling, which we linearly adjust to account for an offset due to different overpass times (Crosson *et al.*, 2012) (Fig. S2).

DGVM for comparison

We use process-based Re simulations from LPJmL as an independent source to compare large-scale spatial Re patterns. The purpose of the comparison is to gain bidirectional confidence in both approaches for regions where they agree and also to identify regions of uncertainty. The LPJmL ecohydrological modeling framework simulates global vegetation and carbon dynamics at 0.5° resolution (Sitch *et al.*, 2003). We force LPJmL with the monthly climatology of the Climate Research Unit's (CRU) TS 3.1 (1901–2009) for temperature, cloudiness and wet days (Mitchell & Jones, 2005) and by the Global Precipitation Climatology Centre's (GPCC) precipitation data (Version 5) (Rudolf *et al.*, 2010). Transient runs follow a 5000-year spinup recycling the first 30 years of input climatology and, in addition, a 390-year agriculture spinup with prescribed historical land use distribution (Fader *et al.*, 2010).

Carbon fluxes (gross primary production, auto- and heterotrophic respiration) and pools (leaves, sapwood, heartwood, storage organs, roots, litter and soil) are mechanistically represented, in direct coupling with the water balance (Gerten *et al.*, 2004) and vegetation dynamics for natural (9 plant functional types, PFT) as well as for agricultural land cover (12 irrigated and rain-fed crop functional types, CFT, and pastures) (Bondeau *et al.*, 2007). Permafrost dynamics along with an updated water-balance implementation are described in Schaphoff *et al.* (2013).

Ra is calculated from the difference of GPP and NPP. Maintenance respiration is calculated individually for each tissue type (leaf, sapwood, and root), based on carbon–nitrogen ratios, air and soil temperature, tissue biomass, and phenology. The temperature sensitivity of Ra follows a modified Arrhenius equation (Lloyd & Taylor, 1994), which describes a decreasing temperature sensitivity with increasing temperature, but parameterization remains constant across biomes and PFTs. Furthermore, 25% of the remainder from GPP and maintenance respiration is substracted as growth respiration, the remainder is NPP. Rh is the sum over carbon emissions from three carbon pools (litter, intermediate, and slow soil

organic matter), for each PFT. Each pool has an assigned turnover rate (0.3, 0.03, and 0.001 a^{-1} at 10 °C, respectively) and decomposition rates are calculated as a function of turnover rate, air and soil temperature, and moisture. The temperature sensitivity of Rh equals the Lloyd & Taylor (1994) dependency. Because RECO and LPJmL employ inherently different approaches to calculate Re, we cannot compare single parameters individually, but only temperature sensitivities and Re estimations itself.

Results

RECO parameterization

In order to aggregate functional biomes, we find that it is inevitable to distinguish three major climate classes TL, TH, and WL, to separate temperature- and water-limited sites. Further, it appears important but less essential to distinguish land cover classes, because responses are not substantially different across land covers. Nevertheless, we can further divide significantly forested and non-forested land cover classes within each climate type. Parameters become insignificant if to further separate agricultural land, due to insufficient amount of data, but driver responses between CRO are GRA are not critically different (Fig. 4). Overall, incorporated Fluxnet data allow to parameterize RECO for six aggregated biomes significantly. Parameter sets for Re_{ref} and Re_{std} and each fitted biome are presented in Tables S3 and S4 in the supplementary information.

Re_{ref} shows robust responses to EVI_{mean} and LST_{mean}, which can be approximated linearly (Fig. 3). EVI_{mean} has positive slopes with steepest increase among GRA/CRO sites. Temperature limitation among TL sites is characterized by a positive Re_{ref} response to LST_{mean}, while all other sites follow a negative slope. Variation among TH-FOR sites, however, is explained to a lower degree compared to other biomes, which adds substantial uncertainty to the overall RECO performance.

Figure 4 illustrates Re_{std} driver responses. The 'sigmoidal' function (Fang & Moncrieff, 2001) exhibits overall best performance to approximate the LST_n response across biomes according to Akaike's Information Criterion (Burnham, 2004). It is flexible enough to match the declining temperature sensitivity that characterizes our data (Fig. 4, Fig. S3). Competing equations and their performance measures are listed in Table S5.

Water-limitation is characterized by a LST_n response that levels off and becomes ambiguous during that period of time. We find low (no) impact of water-limitation on TH (TL) sites, but strong impact on WL sites during the period DoY 136 to 272 (Fig. 4i, k). To account for water stress through LST_{dif}, it was necessary to stratify WL data into dry and non-dry season, because LST_{dif} is only significant during the time of water-limitation (Fig. 4m, o). Here, LST_{dif} explains a large amount of the variation in Re_{std} following a strong negative response (Fig. 4o). The LST_{dif} response at FOR sites is less pronounced compared to GRA/CRO sites (Fig. 4m), because trees are less sensitive to temporary drought impact compared to grass and shrubs, due to deeper rooting and higher water storage capacity (Pereira *et al.*, 2007).

We find EVI is a strong predictor across all climate and land cover types and shows robust responses also outside of the growing season and during periods of water-limitation (Fig. 4). The EVI response appears unsaturated and can be approximated with a linear function. We do not find a time-lag between EVI and Re_{std} at the 8-day scale, which confirms Kuzyakov & Gavrichkova (2010).

MODIS LST correlates closely with Ta ($r_{LSTn} = 0.97$), while LST_n approximates Ta better than LST_d, which shows a systematic bias ($slope_{LSTn} = 0.96$, $slope_{LSTd} = 0.72$). LST_d is affected by light and shadow effects, which limits the ability to predict the baseline temperature (Sims *et al.*, 2008; Wan, 2008). In turn, annual means of LST_d explain more variation in Re_{ref} across all biomes than means of nighttime LST, which can be associated with higher sensitivity of LST_d to surface conditions. Accordingly, we use LST_n as a driver for Re_{std} and mean LST_d for Re_{ref}. Mean EVI of all observations during one year explains less variation in Re_{ref} than mean EVI of springtime observations. The definition of 'springtime' is an empirical finding ($T_{ref} \pm 3$ °C, from first half-year). Further, EVI divided by mean springtime EVI (which we call standardized EVI), explains more variation of Re_{std} across all biomes than plain EVI, because it detrends the EVI response for site-specific slopes. The Snow definition through NDSI > −0.1 (Eqn. 9) outperforms the MODIS snow index (Fig. S1). MODIS IGBP land cover agrees with *in situ* IGBP land cover at 50 of 100 sites, and at 76 of 100 sites for the aggregated classes (Table S2).

RECO evaluation

Final overall model accuracy for 8-day Re predictions based on fivefold cross-validation is $R^2_{Re\_overall} = 0.616$, $RMSE_{Re\_overall} = 1.321$ [g C m^{-2} d^{-1}]. Lowest accuracy is achieved for the mid-latitude TH biome and increases with temperature-limited and water-limited biomes (Fig. 5c, f, i). Overall estimation uncertainty accounts to ± 34.5 percent with little variation across biomes and the model regression slope and MBE do not

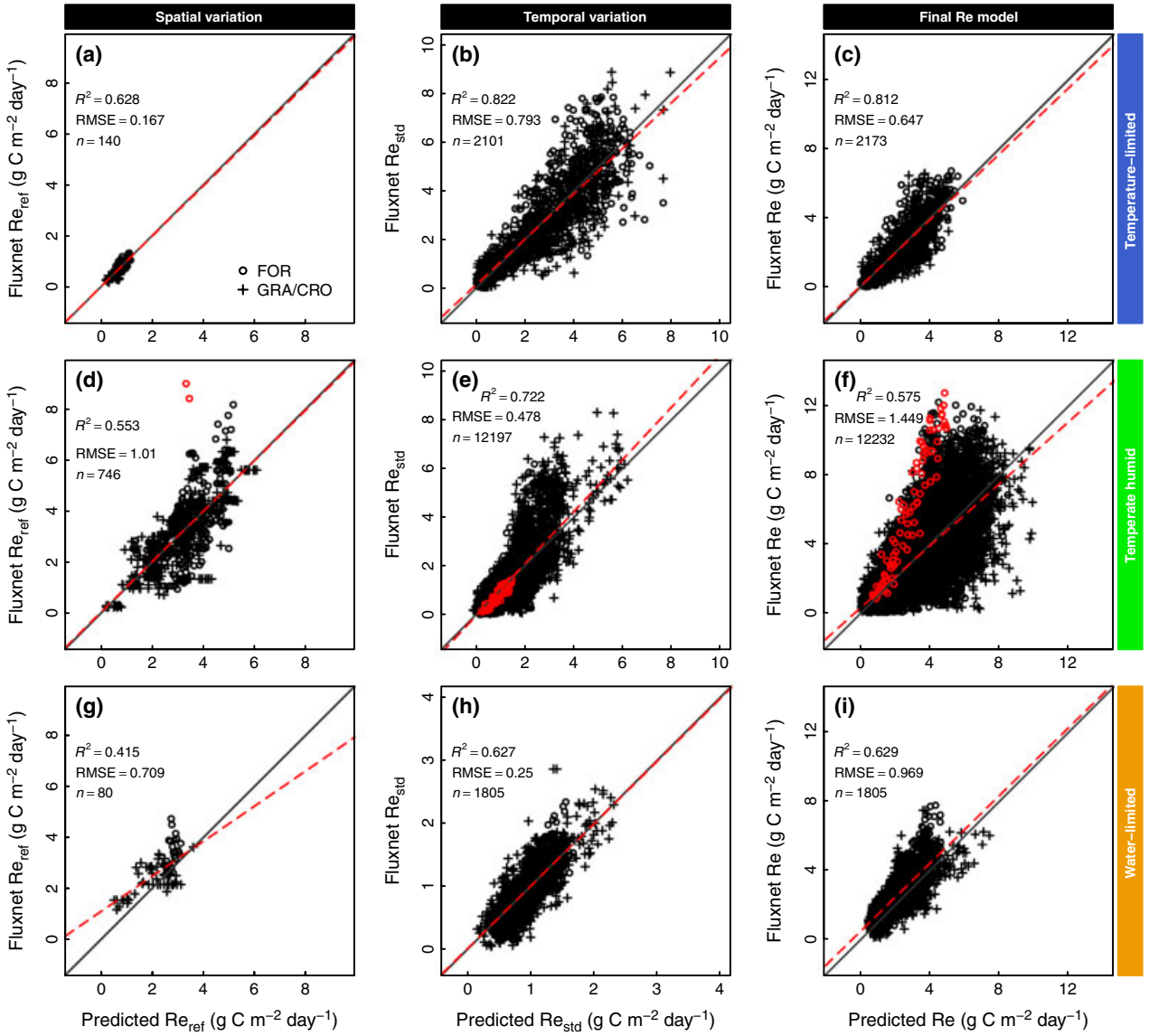

Fig. 5 Model cross-validation results separated for spatial variation (Re_{ref}, first column), temporal variation (Re_{std}, second column) and final Re estimates (third column), against Fluxnet observations. Rows represent climate classes: Temperature-limited, Temperate and humid and Water-limited, respectively. The dashed regression line indicates bias against the 1/1-line. Example site DE-Wet (year 2004, 2005) is colored in red, highlighting the leverage effect of errors in Re_{ref}, to be compared with Fig. 6. Re_{std} values are based on different reference temperatures and thus are plotted at different scales.

indicate a substantial systematic bias [$slope_{overall}$ = 0.91, MBE = 0.051 (g C m^{-2} d^{-1})].

Temporal variability (Re_{std}) is generally explained to a higher degree compared to spatial variability (Re_{ref}) (Fig. 5) ($R^2_{Reref\_overall}$ = 0.682, $R^2_{Restd\_overall}$ = 0.778). Uncertainty in Re_{ref} has a direct leverage effect on final Re estimates (Fig. 5d-f), therefore particularly mid-latitude forest sites (TH-FOR) contribute considerably to overall Re uncertainty, which is a result of the poor TH-FOR response to EVI_{mean} and LST_{mean} (Fig. 3). However, differences in overall Re accuracy between land cover classes are not substantial, only TL-FOR stands out with exceptionally accurate estimates [$R^2_{TL\text{-}FOR}$ = 0.857, $RMSE_{TL\text{-}FOR}$ = 0.593 (g C m^{-2} d^{-1})] (Table S6).

In Figure 6, we show for each biome type time-series for sites with good agreement (left column) face to face with sites revealing typical shortcomings (right column). In general, seasonal variation is tracked robustly across all climate and land cover classes. RECO also shows capacity to reproduce senescence-induced cutback during the dry season in water-limited climates (Fig. 6g) and exhibits reasonable sensitivity to interannual variability. The first of the negative examples

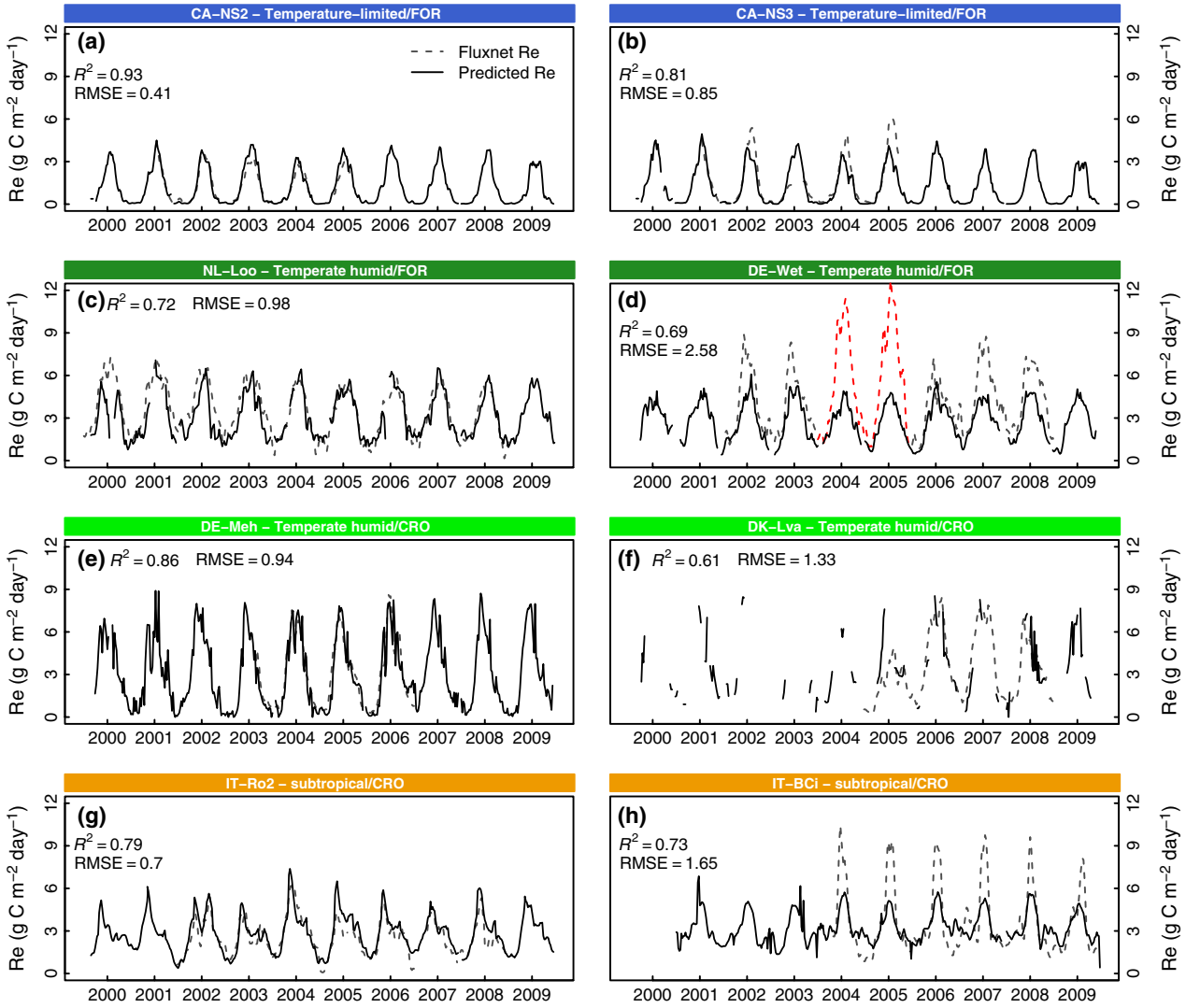

Fig. 6 Time-series plots for Fluxnet (dashed) and modeled (solid) Re at selected sites. For each biome, the left column presents sites with satisfying fits, whereas the right column discloses sites with characteristic problems. (b) and (d) (colored dashed line relates to Fig. 5) highlight potential measuring errors in the Fluxnet record, (f) shows problems due to data availability from the MODIS sensor and (h) discloses insufficient RECO sensitivity to peak respiratory values at a subtropical site after rain events.

(Fig. 6b) shows unusually low summer Fluxnet values in 2003, despite regular signals in EVI and LST and without being documented as disturbance event. Second, Fig. 6d (site DE-Wet, also highlighted in Fig. 5d–f) measures respiration rates well above the average TH forest site, which has been associated with specific micro-meteorological conditions in combination with inhomogeneous and sloped tower footprint (Rebmann *et al.*, 2010). These two examples illustrate the impact of possible errors in the Fluxnet record on the model evaluation, but they also reveal that the model parameterization is robust against such outliers. Figure 6f highlights the problem with data availability from the MODIS sensor. The delivered quality flag rejects a substantial fraction of the 10-year time-series. It is mostly cloud cover that is an crucial issue for missing data, which has a considerable impact on the calculation of annual sums in some regions. As for Fig. 6h, the subtropical cropland site IT-BCi shows a unique pattern: Isolated respiration peaks remain crudely underestimated. Individual rain events after periods of drought have been attributed to increased soil carbon effluxes that can exceed rates under well-watered conditions and for which the temperature dependence temporally gets overridden, the so-called 'Birch-effect' (Xu & Baldocchi 2004, Reichstein & Beer, 2008). These short-term peak events are therefore not to be detected in the EVI and LST signal.

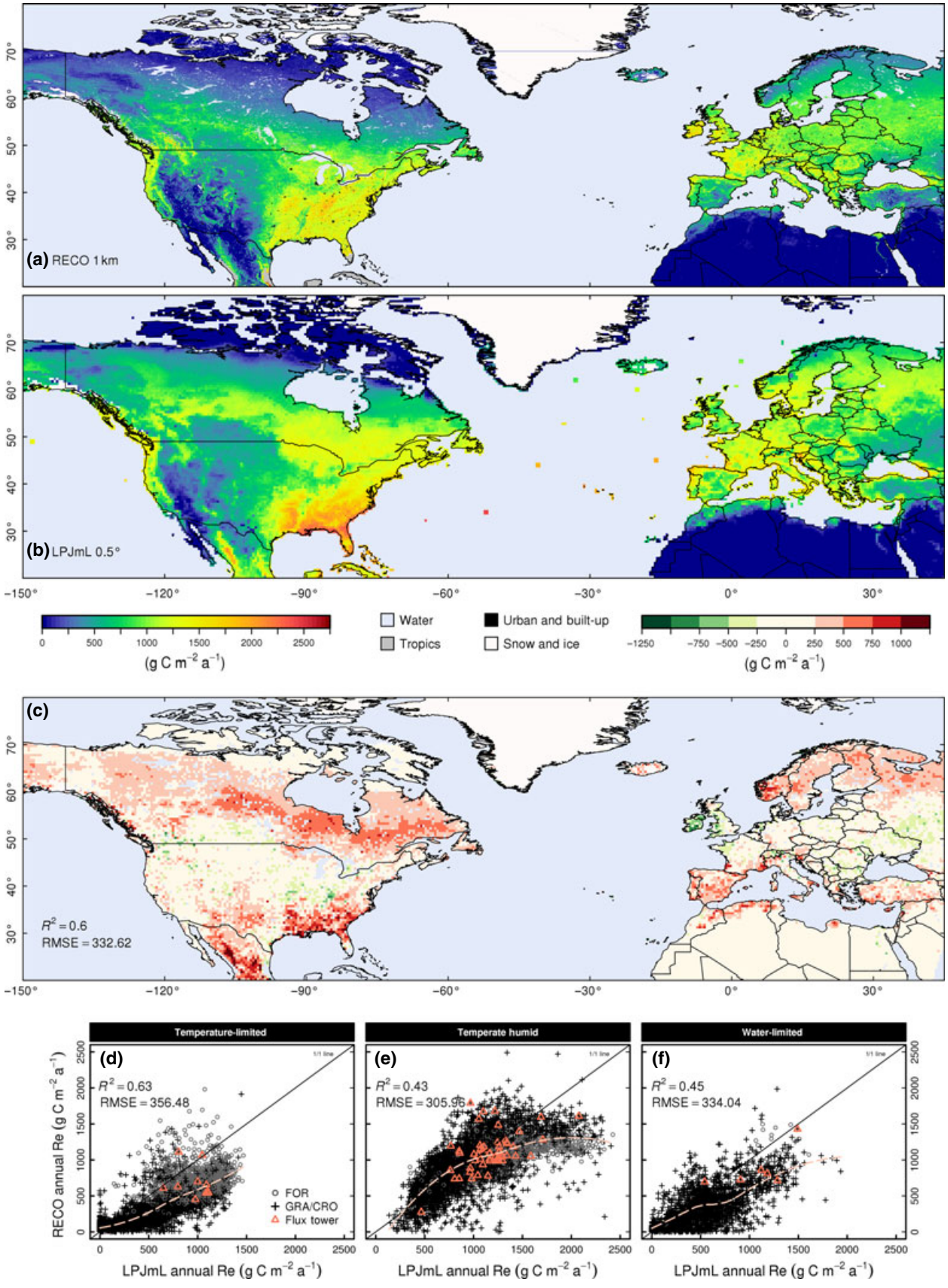
(a) RECO 1 km
(b) LPJmL 0.5°
70°
60°
50°
40°
30°
−150°
−120°
−90°
−60°
−30°
0°
30°
0
500
1000
1500
2000
2500
(g C m−2 a−1)
Water
Tropics
Urban and built-up
Snow and ice
−1250
−750
−500
−250
0
250
500
750
1000
(g C m−2 a−1)
(c)
R2 = 0.6
RMSE = 332.62
Temperature-limited
Temperate humid
Water-limited
(d)
R2 = 0.63
RMSE = 356.48
(e)
R2 = 0.43
RMSE = 305.96
(f)
R2 = 0.45
RMSE = 334.04
1/1 line
FOR
GRA/CRO
Flux tower
RECO annual Re (g C m−2 a−1)
LPJmL annual Re (g C m−2 a−1)

Fig. 7 2003 annual sums of Re, predicted by RECO with 1 km resolution (a) and simulated by LPJmL with 0.5° resolution (b). Urban and Built-up and Tropics land cover classes only apply to (a). A difference map at 0.5° grid is shown in (c) and scatter-plots of RECO versus LPJmL annual sums for all pixels from the displayed extent are plotted by climate type in (d)–(f). Dashed lines indicate polynomial bias curve.

Spatial pattern comparison with LPJmL

Re annual sums for 2003 across North America and Europe, predicted by RECO and simulated by LPJmL, are illustrated in Fig. 7. Both methods estimate similarly characteristic large-scale spatial patterns. For example, the distinct west-east soil moisture gradient throughout North America with peak values at the south and south-east coastline, the US south-west desert regions and the North-American west coast and its patchy patterns around British Columbia are modeled similarly. Spatial patterns across Europe are also reasonably well in agreement, for example, high values in western France to low values along the European Alps and the elevated footprint of the Carpathians to the pronounced south-east border of the Black Sea and the greening of the Nile delta.

A difference map of LPJmL minus RECO annual sums at the 0.5° grid (Fig. 7c) reveals specific regions of uncertainty. The overall agreement between both models for all pixels is $R^2 = 0.6$, RMSE = 332.62 [g C m^{-2} a^{-1}]. While mid-latitude regions between 40°N and 55°N are well in agreement, LPJmL simulates consistently higher values in boreal and high-latitude regions in Canada and north-eastern Europe, but also in subtropical regions in south-eastern US and Mexico and along the coastline of the Mediterranean Sea. One of the rare areas where RECO predicts substantially higher values than LPJmL is Ireland and south-western UK. Mean biased error (MBE) between RECO and LPJmL accounts to −174.4 [g C m^{-2} a^{-1}], indicating a consistent over-prediction by LPJmL. Figure 7 d-f show scatter-plots of RECO versus LPJmL pixels for the above presented map, including Flux tower locations. The mean error is highest among TL and WL biomes and decreases where tower distribution is dense, that is, in the TH biome (despite higher annual sums). Importantly, regions where both models diverge most significantly are represented by Flux towers at least to some degree. Regions with no tower representation mostly have very low annual sums in TL and WL, where in turn both models are sufficiently in agreement. Given this, Fluxnet towers appear to form a valid reference tool and to be appropriate for up-scaling to the study region.

Taking Fluxnet sites for reference, LPJmL annual errors exceed those from RECO by one-quarter ($RMSE_{LPJmL\_annual}$ = 396.7 [g C m^{-2} a^{-1}], and $RMSE_{RECO\_annual}$ = 305.8 [g C m^{-2} a^{-1}], resp.). But most importantly, LPJmL shows systematic positive bias throughout all investigated biomes. MBE for annual sums accounts to MBE_{LPJmL} = −153 and MBE_{RECO} = 21.3 [g C m^{-2} a^{-1}], respectively. Ordered by latitude, Fig. 8 marks mean annual residuals for each site. The LPJmL trend-line across latitudes remains with negative values (positive bias) for all but a few central European sites. Carbon efflux is simulated most excessively at the TL biome (CA-NS2/3, FI-Hyy, SE-Fla, FI-Sod, FI-Kaa) and sites among the south-east US (US-KS2, US-SP3, US-Goo). The trend of RECO annual residuals is located reasonably close to zero for all biomes, except for the south-east US, where RECO underestimates annual sums as much as LPJmL overestimates, which renders this as a region of specific uncertainty. Interestingly, IE-Dri and UK-Esa represent the region where RECO predicts higher values than LPJmL, but Fig. 8 indicates that this is due to underestimation in LPJmL.

Evaluation of mean monthly estimates is shown in Figure 9. While the monthly bias pattern is consistent with the bias of annual sums, mean monthly estimates show considerably higher accuracy in both models (Fig. 8, 9). RECO achieves smaller mean monthly errors compared to LPJmL ($RMSE_{RECO}$ = 1.22 and $RMSE_{LPJmL}$ = 1.59 [g C m^{-2} d^{-1}], resp.), which shows positive bias across all biomes, most pronounced for TL sites ($slope_{TL}$ = 0.45, $slope_{TH}$ = 0.72, $slope_{WL}$ = 0.89). In comparison, RECO shows very small bias in all three fitted biomes ($slope_{TL}$ = 0.97, $slope_{TH}$ = 0.92, $slope_{WL}$ = 1.03). The error between RECO and LPJmL at tower pixels is 1.42 [g C m^{-2} d^{-1}], which indicates that LPJmL agrees better with RECO than with tower data. Interestingly, this value stays remarkably stable if all pixel are included ($RMSE_{RECO\text{-}LPJmL\text{-}all}$ = 1.41 [g C m^{-2} d^{-1}]).

Evidently, residuals increase with increasing Re over the growing season in both models (Fig. 9c, d). RECO residuals indicate an underestimation during WL summer months, but no distinct seasonal pattern for the other biomes. LPJmL residuals show a considerable seasonal pattern with distinct negative median residuals during the growing season with TH and TL biomes. Median residuals in the TL biome exceed -2 [g C m^{-2} d^{-1}] from June to September.

Discussion

RECO evaluation

The RECO model demonstrates that Fluxnet Re observations can be estimated with an applicable degree of

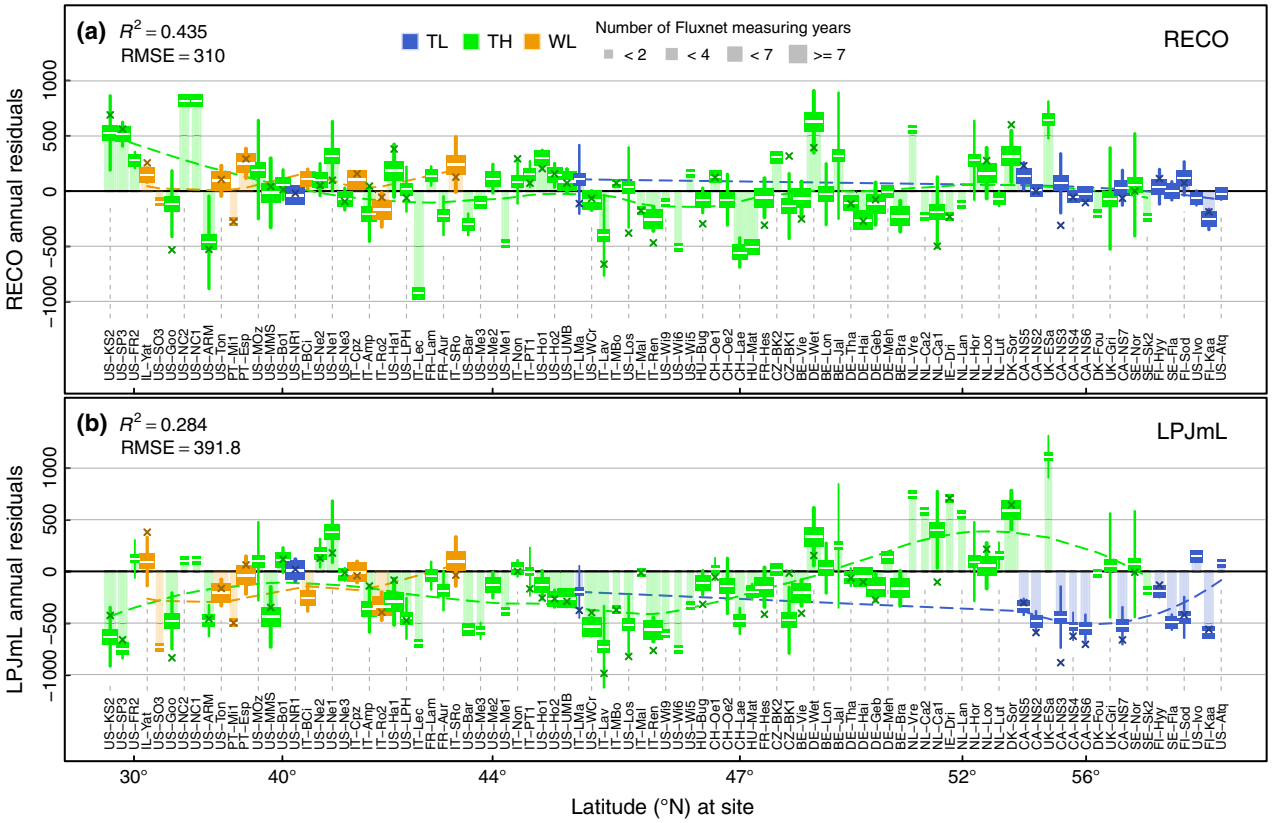

Fig. 8 Mean site-level residuals of annual sums (2000–2009), (a) RECO and (b) LPJmL, ordered by latitude. Vertical solid lines indicate the standard deviation, box sizes increase with number of available measuring years. Values for year 2003 are indicated with '×' to represent values from the map in Fig. 7. Dashed lines indicate trends.

accuracy across major global biomes using only satellite remote sensing data. Its semi-empirical approach proves instrumental in capturing a high amount of spatio-temporal variability. The definition of Re_{ref} as the reference respiration rate factor is key to segregate temporal and spatial variations, which is crucial to designing an operational model, because site characteristics are associated with Re_{ref} and temporal variation is standardized across sites. Reichstein *et al.* (2007) and Migliavacca *et al.* (2011) present such an approach at the plot scale, and Yuan *et al.* (2011) provides a global map of Re_{ref} based on GPP estimates from a light use efficiency model. But to our knowledge, this concept has not been subject to an operational remote sensing-based study applicable to large scales at the 1 km resolution.

Incorporated drivers serve as higher level proxies for more complex underlying sub-processes. For example, at very high latitude sites, LST_n explains more variation in Re than *in situ* air temperature, which is remarkable, since LST is a space-borne product with a considerable bias against Ta measurements (RMSE = 2.84 °C). The LST product is specifically suitable for monitoring ecosystem conditions and stresses, in that it is not only a proxy for temperature but also for other processes such as vapor pressure deficit (VPD). For example, reduced stomatal conductance, that is, higher VPD, and reduced vegetation cover during periods of drought cause elevated daytime LST (Hashimoto *et al.*, 2008; Sims *et al.*, 2008), which hence characterizes ecosystem states more generally. Moreover, plant productivity is affected by water stress, and associated senescence effects cause reduction in vegetation canopy chlorophyll content, which can be observed by vegetation indices. This explains why EVI significantly contributes to tracking Re during periods of water stress. At the pixel-scale, EVI is also capable to accounting for disturbances and management to a certain degree. EVI contributes to Re_{std} estimates as a high-level proxy for plant productivity, plant physiognomy and plant water stress. Compared to previous remote sensing-based studies (Vourlitis *et al.*, 2003; Gilmanov *et al.*, 2005; Yamaji *et al.*, 2007; Schubert *et al.*, 2010), we directly account for plant water stress through LST_{dif} which extends the operational area to semiarid climates. Most existing approaches also exploit the temperature

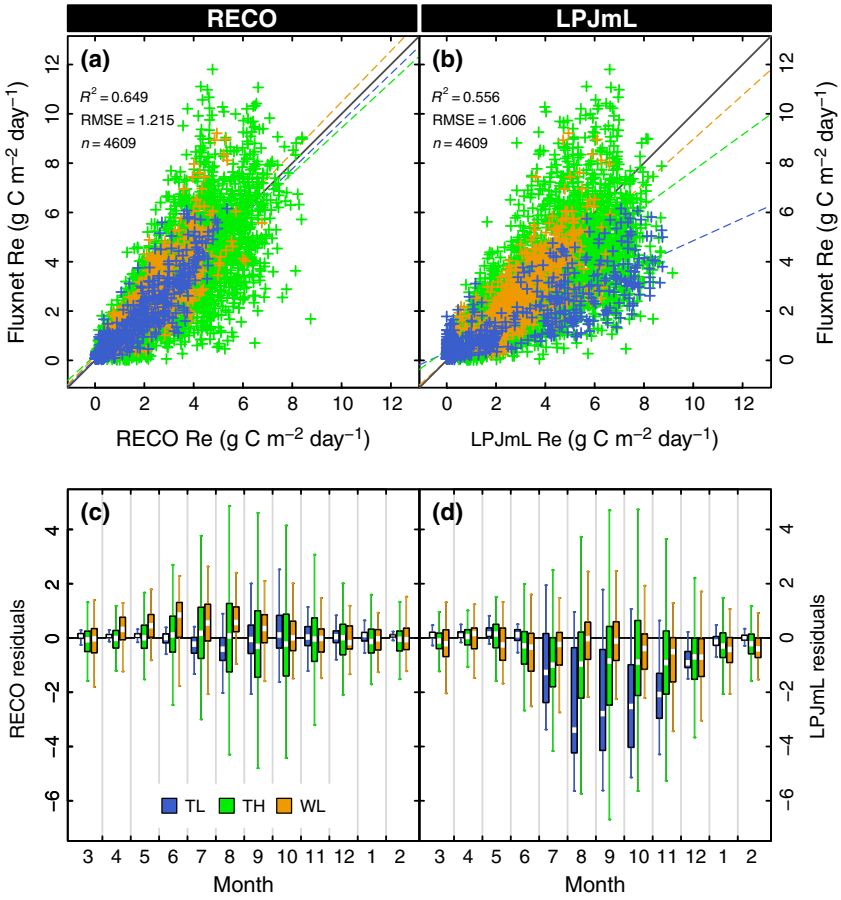

Fig. 9 Evaluation of the RECO (left-hand column) and LPJmL (right-hand column) against Fluxnet data for monthly averages (first row) and seasonal variation of mean monthly residuals, as box-and-whisker plots (second row, whiskers are set to 1.5 inter quartile range). The solid line in (a) and (b) is the 1/1 line, dashed lines indicate the bias. TL, TH and WL abbreviate Temperature-Limited, Temperate and Humid and Water-Limited, respectively.

dependence of respiration during periods of water limitation, which we have shown to be ambiguous. Although all RECO predictor variables are selected empirically, we follow physiological dependencies, which marks RECO as a semi-empirical approach.

Overall, RECO accuracy is on a par other recent approaches: Kimball *et al.* (2009), for example, estimated Re for boreal and Arctic biomes with a remote sensing-based model accounting for soil moisture (AMSR-E data, currently out of order, as of September 13, 2013) and three different soil carbon pools. They achieve mean site-level accuracy of $R^2 = 0.54$ and RMSE = 0.73 [g C m^{-2} d^{-1}]. For that biome, we calculate: $R^2 = 0.82$ and RMSE = 0.58 [g C m^{-2} d^{-1}]. Further, overall RECO results are close to the *in situ* 8-day study by Migliavacca *et al.* (2011). They found an overall fit of $R^2 = 0.72$ and mean RMSE = 1.06 [g C m^{-2} d^{-1}], while we calculate for a very similar data set, but based on remote sensing input: $R^2 = 0.69$ and mean RMSE = 1.24 [g C m^{-2} d^{-1}]. While Migliavacca *et al.* achieve a higher degree of accuracy in annual sums, the additional uncertainty in our study might be due to the spatial mismatch between tower footprint and satellite pixel. Jung *et al.* (2011) calculate monthly values with performance measures of: $R^2 = 0.69$ and RMSE = 1.04 [g C m^{-2} month^{-1}] which slightly exceed our values [$R^2 = 0.65$ and RMSE = 1.21 (g C m^{-2} month^{-1})].

We calculate Re_{ref} on a yearly basis to account for interannual variation, disturbances, and trends. Due to its multiplicative design (Eqn. 3), errors in Re_{ref} have a distinct leverage effect on final Re estimates. This is particularly the case among TH sites, where model residuals are mainly induced by considerable uncertainty associated with Re_{ref}. A temporally static Re_{ref}, however, leads to lower overall accuracy measures (not shown). In general, annual means of EVI and LST explain a sufficient amount of the variability in Re_{ref} across non-tropical biomes. Re_{ref} depends strongly on photosynthesis (e.g., Janssens *et al.*, 2001; Yuan *et al.*, 2011) and thus has often been modeled based on LAI

observations (Hibbard *et al.*, 2005; Lindroth *et al.*, 2008; Migliavacca *et al.*, 2011). But in our study, EVI and mean EVI consistently outperform LAI and mean LAI, respectively. We assume that mean EVI observations can roughly account for substrate availability and biomass and also to a low degree for labile soil carbon pools. However, we expect that more accurate information on slow soil carbon pools, substrate availability, and soil structure would considerable contribute to better explaining variations in Re_{ref} between sites and years. We investigated biomass products from *in situ* and remote sensing-based data (Blackard *et al.*, 2008) and also soil carbon data (Global Soil Data Task, 2000), without finding a significant contribution (not shown). Current advances in remote sensing of terrestrial biomass (e.g., Bellassen *et al.*, 2011; Saatchi *et al.*, 2011) could contribute to reduce uncertainty. The goal of this study, however, was to develop a single-sensor operational product that fits into the existing MODIS product family in terms of spatio-temporal resolution, to allow the combination with existing GPP products.

A positive relation between Re_{ref} and mean LST is an indicator for temperature limitation (Fig. 3). The negative dependency between Re_{ref} and mean LST among sites that are not temperature-limited can be associated with two different reasons. First, the phenological state at temperature T_{ref} varies between sites (i.e., sites with lower mean annual temperature are more advanced into the growing season than warmer sites and thus baseline respiration is higher). Second, as it has been shown frequently, the apparent temperature sensitivity decreases with increasing mean temperature (see following paragraph). Mean LST is sensitive to elevation gradients and the climate classification only accounts for elevation at a large scale. Nevertheless, the response to Re_{ref} is reasonably strong.

The true temperature sensitivity of respiratory processes and the question if it varies systematically between ecosystems and over time is still under debate (Davidson & Janssens, 2006; Gu *et al.*, 2008; Kirschbaum, 2010; Mahecha *et al.*, 2010; Yvon-Durocher *et al.*, 2012). The well-known exponential Q_{10} function (Black *et al.*, 1996) is characterized by a constant Q_{10} over space and time, where Q_{10} is the factor by which respiration multiplies in response to a 10° temperature increase. Lloyd & Taylor (1994) show that an exponential increase underestimates low and overestimates high respiration measurements and they present a modified Arrhenius type function with a declining Q_{10} at higher temperatures. More flexible s-shaped functions were developed (Kirschbaum, 1995; Fang & Moncrieff, 2001; Del Grosso *et al.*, 2005) to even better meet field measurements and it has been shown that the apparent temperature sensitivity varies spatially with higher sensitivities among colder climates and lowest values among deserts (e.g., Tjoelker *et al.*, 2001; Zhou *et al.*, 2009; Chen *et al.*, 2010). Variations in Q_{10} are generally attributed to temperature acclimation during the season and limitations by water and biomass, as substrate availability decreases with increasing temperature (Ryan, 1991; Raich & Schlesinger, 1992). On the contrary, Yvon-Durocher *et al.* (2012) were recently able to show that the short-term temperature sensitivity between different ecosystems is very similar and Schindlbacher *et al.* (2009) concludes that root autotrophic and soil heterotrophic respiration responded equally to temperature. Moreover, Reichstein & Beer (2008) attributed the Q_{10} decline at higher temperatures to interactions with soil moisture limitations, while Mahecha *et al.* (2010) circumvented those confounding effects and concluded with a spatio-temporally static Q_{10} of 1.4. However, despite the discussion on the true temperature sensitivity, at the ecosystem level the Lloyd & Taylor function remains one of the most common temperature sensitivities in recent empirical and process-based models (e.g., Sitch *et al.*, 2003; Reichstein *et al.*, 2007; Schubert *et al.*, 2010; Migliavacca *et al.*, 2011).

In our study, we examine large-scale ecosystem-level 8-day average data in which we cannot circumvent entirely limiting factors. We account for the finding that temperature sensitivity changes across different time

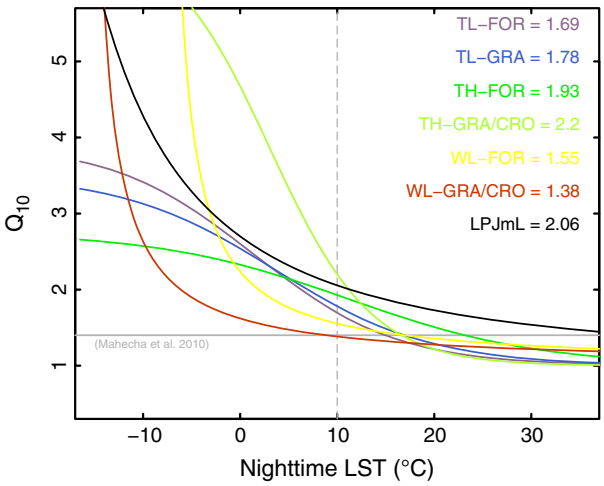

Fig. 10 Q_{10} temperature sensitivities over the range of nighttime LST for all six fitted biomes and for LPJmL, respectively. Q_{10} values in the legend are values at 10 °C. Gray line indicates the Q_{10} estimate from Mahecha *et al.* (2010). The black line represents the Lloyd & Taylor temperature response (employed in LPJmL), but linearly adjusted to match nighttime temperatures. Note that RECO temperature responses are based on different T_{ref} values (TL = 0 °C, TH = 12 °C, WT = 13 °C), therefore Q_{10} values between these three classes are not directly comparable.

scales (Kirschbaum, 2010; Yvon-Durocher *et al.*, 2012) in that we relate the long term response (Re_{ref}, annual) to mean LST_d and the short-term response (Re_{std}, weekly) to short-term variations in LST_n. We confirm that the fitted apparent short-term temperature sensitivity declines at higher temperatures (Fig. 10) and we find that it is approximated best by the 'sigmoidal' function (Table S5). Although we find spatial differences in fitted Q_{10} between biomes, they are not substantial, with exception of the TH-GRA/CRO fit (issue with climate classification, see below). The general picture is that Q_{10} at 10 °C has lowest values at WL sites and increases with TH and TL sites (Fig. 10) and they are within the range of previously reported values (Zhou *et al.*, 2009; Bond-Lamberty & Thomson, 2010; Yvon-Durocher *et al.*, 2012). LPJmL shows consistently higher Q_{10} values than RECO beyond 10 °C LST_n (Fig. 10), which has a considerable effect on Re estimates at the upper temperature range.

Above all discussions on the temperature sensitivity, our study shows that uncertainty in the approximation of the temperature sensitivity only contributes a small fraction to the overall RECO uncertainty. The temperature responses are mostly well constrained and overall model results from different temperature functions are very similar (Table S5). We point out that it is the uncertainty associated with limiting factors to the reference respiration rate that triggers considerable errors and remains a crucial issue.

Land cover types are aggregated to only two functional classes because it was crucial to divide the three climate classes first and the number of available sites remaining within each climate class restricts finer land cover separation. Nevertheless, accuracy in Re_{std} estimates is very high ($R^2 = 0.78$) and does not appear to be hampered by land cover aggregation. The LST_n response is smoothed across sites and land covers and temperature sensitivities do not vary much (Fig. 10). Forested and non-forested land covers are divided because of different EVI and LST_{dif} responses, but further separation of agricultural land is not significant with the data available. Using static land cover information (aggregated for the years 2001–2005) introduces errors for regions with extensive land cover change. Yet, we reduce uncertainties in the MODIS land cover product by aggregating classes to broader functional types.

More importantly, the coarse climate class stratification limits better Re standardization with sharper driver responses. Especially, the TH class spans a wide range from the tropical border in southern US to temperature-limited regions in Canada. Therefore, the phenological state within the growing season at a given temperature, T_{ref}, varies and thus the reference rate at T_{ref} does not standardize Re equally at each site. For example, Figure 4 g discloses a cloud of very high Re_{std} values around 20 °C LST, which follow an exceptionally high temperature dependency. This is an effect of T_{ref} being too early in the growing season and therefore confounds the standardization, which leads to unusually high Q_{10} values for that biome (Fig. 10). Lower T_{ref} values, however, produce negative effects at the other end of the temperature range.

Parameter estimation is weighted by uncertainty, thus observations with small uncertainty have larger influence. This ensures that summer peak observations do not bias regression parameters, but accordingly they are predicted less accurately. Nonetheless, it is a general quality feature to achieve a reliable base-flow and reliable seasonal variation, rather than to match peak carbon efflux events. Residuals increase during the growing season, yet with no distinct bias (Fig. 9c). Further, we assume that autotrophic and heterotrophic shares are constant over the season, which is disputed (Falge *et al.*, 2002; Davidson *et al.*, 2006b). GPP and Ra decline in late summer, and Rh is amplified due to increased litter fall and precipitation. A partitioning of these processes by means of remote sensing appears currently not feasible. Also, RECO appears to be valid only for the equilibrium state since we do not account for feedback effects and slow soil carbon pools. We aim to establish a short-term monitoring tool for the current static state, for which it is not necessarily required to account for different carbon pools and soil turnover times (Migliavacca *et al.*, 2011).

Besides these shortcomings of the RECO approach, Fluxnet measurements, especially of Re, contain considerable random and systematic errors. They can be attributed to limitations to the methodology and to differences in data processing. Random errors increase with magnitude of the flux (Richardson *et al.*, 2006b; Richardson *et al.*, 2008). Systematic errors arise from uncertainty in the partitioning methodology of NEE (Reichstein *et al.*, 2005; Lasslop *et al.*, 2010) and, more importantly, to advection losses at low-turbulence conditions, in spite of the applied u*-filtering (Aubinet, 2008; Williams *et al.*, 2009). They mostly occur at nighttime and tend to produce underestimation in Re measurements (Massman & Lee, 2002; Baldocchi, 2003), which is important to point out since it might have contributed to the fact that the here presented study, as well as Jung *et al.* (2011), both result in Re estimates that are considerably lower compared to DGVM and literature values. However, the quantification and correction of systematic errors in the Fluxnet record is not trivial and critically remains a problem.

Moreover, Fluxnet sites represent major biomes with a sufficient number of sites to allow for stratified

parameter estimates. A dense network is established among mid- and high latitudes at the northern hemisphere, but there is still a measurement gap for semi-arid, arid, and tropical climates and for the southern hemisphere in general (Baldocchi, 2008). We only have data available for two sites in the tropics, where we can explain spatial variation to some degree, but predictors remain insignificant in accounting for seasonal variation (Samanta *et al.*, 2012). Although it would be feasible in principle to extrapolate the model parameterization to the global scale, we therefore restrict our analysis to North America and Europe (where training sites are located). The carbon budget of the tropics is assumed to be close to neutral and the global terrestrial carbon sink is generally attributed to high-latitude extra-tropical areas (Pan *et al.*, 2011), regions that are expected to be highly vulnerable to environmental change and also show large year-to-year variability (Canadell *et al.*, 2007; Le Quéré *et al.*, 2009).

DGVM comparison

We demonstrated that RECO has a negligible bias against Fluxnet Re observations and mean errors are smaller or comparable to previous studies. Furthermore, we show that Fluxnet towers are reasonably distributed over the range of annual sums calculated by RECO and LPJmL, which supports the assumption that incorporated Fluxnet data are representative and allow for upscaling. Moreover, RECO is able to reproduce large-scale spatial Re patterns disclosed by LPJmL, across all investigated biomes. Hence, we conclude that RECO is sufficient for up-scaling Re estimates to the continental-scale. Nonetheless, considerable differences exist in Re magnitudes between LPJmL and RECO, which merit further discussion.

Throughout this analysis, LPJmL simulates higher Re estimates compared to RECO and Fluxnet data. Here, we consider three possible explanations: (i) systematic bias in the Fluxnet measurement technique, (ii) inadequate parameterization of LPJmL, including the temperature sensitivity, and less likely, (iii) uncertainty due to scaling effects and climate and soil input data to LPJmL.

(i) Previous studies found systematic errors in the Fluxnet record due to advection losses to be significant. Jung *et al.* (2011) scale Fluxnet data to the global scale and calculate annual Re values 5–10% lower than previously thought, which they attribute to biased sampling and disturbance events. Kucharik *et al.* (2006) evaluate the IBIS DGVM, which employs the same temperature sensitivity as LPJmL, at Fluxnet sites and find a consistent overestimation in annual Re estimates at all three investigated sites of 16% to 29%. They associate errors with underestimation of observed nighttime Re at tower sites and also to a too pronounced temperature sensitivity of stem, root and leaf. Findings by Hanson & Amthor (2004) are similar; they find that the mean annual Re simulated by 10 independent models exceed observations by 27%. The above findings are in line with our results and thus we consider systematic errors in the Fluxnet record to contribute to the 'shifted baseline' between LPJmL and RECO. Yet, the associated uncertainty remains to be quantified.

Contradictory to this hypothesis is that model discrepancies show a distinct spatial pattern (Fig. 7c) and they are especially associated with high-level observations (Fig. 7d–f). It is particularly the boreal zone that stands out with a clear offset against Fluxnet data (Figs 8b, 9b, slope = 0.45 between Fluxnet and LPJmL), while mid-latitude continental regions are well in agreement.

(ii) In Figure 10, we show that the temperature sensitivity of LPJmL is generally higher than in RECO, which has a particularly strong effect at the upper temperature range. We consider this a possible reason that LPJmL shows higher estimates especially with high-level observations. The temperature sensitivity implemented in LPJmL is a well-known and commonly applied dependency, while many other DGVMs employ an even higher Q_{10} of 2 (Friedlingstein *et al.*, 2006). But recent studies suggest it could be overestimated (Mahecha *et al.*, 2010), while practical conclusions for the ecosystem level remain difficult to draw (Reich, 2010; Graf *et al.*, 2011). DGVM parameterization of the temperature sensitivity is critically important to study the climate change impact on the resilience of the carbon cycle and soil carbon stocks in particular (Jones *et al.*, 2003). However, it is not only the temperature sensitivity that constraints Re simulations in LPJmL and biotic factors influencing the temperature dependence are as important (Davidson *et al.*, 2006a; Bond-Lamberty & Thomson, 2010). Various process interactions between photosynthesis, precipitation and temperature and model assumptions, especially on turnover rates of soil carbon pools and soil parameters, determine Re simulations and conceal the mere dependency on temperature (Zaehle *et al.*, 2005). But a mechanistic understanding of complex process interactions is still lacking (Davidson *et al.*, 2006a). We argue that it is inadequate to associate model discrepancies with temperature sensitivities only. But it merits a further study to conduct a thorough parameter sensitivity analysis in order to identify those parameters in LPJmL that induce the apparent discrepancies. Moreover, LPJmL simulates higher global annual Re sums (129.68 ± 0.9 Pg C a^{-1}, 2000-2009) compared to recent estimates of 103 (Yuan *et al.*, 2011), 96 ± 6.0 (Jung *et al.*, 2011), and 119.6 Pg C a^{-1} (Denman *et al.*, 2007).

The finding that the here presented methods diverge fundamentally in the boreal zone is of critical importance to the modeling of the future resilience of the global carbon cycle. These high-latitude regions are expected to be specifically vulnerable to climate change impacts due to large carbon stocks and above average temperature increase (Dorrepaal *et al*., 2009; Bond-Lamberty & Thomson, 2010). Evidently, RECO cannot account for climate change impacts on slow carbon pools, but it provides a crucial measure to reveal current respiratory patterns and thus can help to calibrate DGVM estimates better, in order to increase our confidence in DGVM-simulated future climate change impacts.

We point out that the comparison of such intrinsically different models is only partly conclusive. For instance, comparing pixels of 1 km and 0.5° resolution involves errors due to scaling effects. RECO is trained and validated on Fluxnet data, thus it is clear that such a model will predict plot scale measurements better than a global process-based model not being calibrated to site-specific conditions. Gap-filling in MODIS and Fluxnet annual sums induce additional errors, but since the bias pattern is consistent across time aggregation, we neglect this point.

(iii) It remains difficult to assess uncertainty from climate input, but precipitation is generally the most uncertain variable. To test the associated uncertainty, we ran LPJmL with a competing precipitation data set (modified version of Oesterle *et al*., 2003), which generates a RMSE = 88 [g C m^{-2} a^{-1}]. This is a considerable fraction of the 333 [g C m^{-2} a^{-1}] between LPJmL and RECO.

Notwithstanding remaining shortcomings of the RECO methodology, RECO forms an operational, cross-validated, and unbiased approach to estimating continental-scale Re. It can readily be combined with existing GPP products (e.g., Sims *et al*., 2008) to calculate per-pixel NEE at 1 km and 8-day resolution. Since the steadily growing MODIS data pool now exceeds a decade of coverage, longer term trend analyses start to be feasible. Pending sufficiently accurate global estimates of terrestrial carbon fluxes, this study advances knowledge of local-scale spatio-temporal Re variability. We complement independent process-based estimates and reveal a critical gap among high-latitude regions. Underlying reasons that are contributing to such differences need to be further identified to reduce uncertainty in future projections of the global carbon cycle feedback to climate change impacts.

Acknowledgements

We are thankful for the freely available Flux data at http://www.fluxnet.ornl.gov, which are subject to Fluxnet Data Fair Use Policies and we are grateful for the convenient and free provision of MODIS data at http://daac.ornl.gov/MODIS/modis.html. Sibyll Schaphoff, Steven W. Running and two anonymous reviewers are kindly acknowledged for additional comments. We also acknowledge the European Communities' Seventh Framework Program (Climafrica project, grant no. 244240).

The authors declare no conflict of interest.

References

Aubinet M (2008) Eddy covariance CO_2 flux measurements in nocturnal conditions: An analysis of the problem. *Ecological Applications*, **18**, 1368–1378.

Aubinet M, Grelle A, Ibrom A *et al*. (2000) Estimates of the Annual Net Carbon and Water Exchange of Forests: the EUROFLUX Methodology. *Advances in Ecological Research*, **30**, 113–175.

Bahn M, Janssens IA, Reichstein M, Smith P, Trumbore SE (2010) Soil respiration across scales: towards an integration of patterns and processes. *The New Phytologist*, **186**, 292–296.

Baldocchi D (2003) Assessing the eddy covariance technique for evaluating carbon dioxide exchange rates of ecosystems: past, present and future. *Global Change Biology*, **9**, 1–14.

Baldocchi D (2008) TURNER REVIEW No. 15 "Breathing" of the terrestrial biosphere: lessons learned from a global network of carbon dioxide flux measurement systems. *Australian Journal of Botany*, **56**, 1–26.

Baldocchi D, Falge E, Gu L *et al*. (2001) FLUXNET: a New Tool to Study the Temporal and Spatial Variability of Ecosystem-Scale Carbon Dioxide, Water Vapor, and Energy Flux Densities. *Bulletin of the American Meteorological Society*, **82**, 2415–2434.

Beer C, Reichstein M, Tomelleri E *et al*. (2010) Terrestrial gross carbon dioxide uptake: global distribution and covariation with climate. *Science*, **329**, 834–838.

Bellassen V, Delbart N, Le Maire G, Luyssaert S, Ciais P, Viovy N (2011) Potential knowledge gain in large-scale simulations of forest carbon fluxes from remotely sensed biomass and height. *Forest Ecology and Management*, **261**, 515–530.

Black TA, Hartog G, Neumann HH *et al*. (1996) Annual cycles of water vapour and carbon dioxide fluxes in and above a boreal aspen forest. *Global Change Biology*, **2**, 219–229.

Blackard J, Finco M, Helmer E *et al*. (2008) Mapping U.S. forest biomass using nationwide forest inventory data and moderate resolution information. *Remote Sensing of Environment*, **112**, 1658–1677.

Bondeau A, Smith PC, Zaehle S *et al*. (2007) Modelling the role of agriculture for the 20th century global terrestrial carbon balance. *Global Change Biology*, **13**, 679–706.

Bond-Lamberty B, Thomson A (2010) Temperature-associated increases in the global soil respiration record. *Nature*, **464**, 579–582.

Burnham KP (2004) Multimodel Inference: understanding AIC and BIC in Model Selection. *Sociological Methods & Research*, **33**, 261–304.

Cai G, Xue Y, Hu Y *et al*. (2007) Soil moisture retrieval from MODIS data in Northern China Plain using thermal inertia model. *International Journal of Remote Sensing*, **28**, 3567–3581.

Canadell J, Pataki D, Gifford R *et al*. (2007) Saturation of the terrestrial carbon sink. In: *Terrestrial Ecosystems in a Changing World* (eds Canadell J, Pataki D, Pitelka L), pp. 59–78. Berlin Heidelberg, The IGBP Series, Springer-Verlag.

Chen S, Huang Y, Zou J *et al*. (2010) Modeling interannual variability of global soil respiration from climate and soil properties. *Agricultural and Forest Meteorology*, **150**, 590–605.

Coll C, Wan Z, Galve JM (2009) Temperature-based and radiance-based validations of the V5 MODIS land surface temperature product. *Journal of Geophysical Research*, **114**, D20102.

Cramer W, Bondeau A, Woodward FI *et al*. (2001) Global response of terrestrial ecosystem structure and function to CO 2 and climate change: results from six dynamic global vegetation models. *Global Change Biology*, **7**, 357–373.

Crosson WL, Al-Hamdan MZ, Hemmings SNJ, Wade GM (2012) A daily merged MODIS Aqua–Terra land surface temperature data set for the conterminous United States. *Remote Sensing of Environment*, **119**, 315–324.

Davidson EA, Janssens IA (2006) Temperature sensitivity of soil carbon decomposition and feedbacks to climate change. *Nature*, **440**, 165–173.

Davidson EA, Janssens IA, Luo Y (2006a) On the variability of respiration in terrestrial ecosystems: moving beyond Q10. *Global Change Biology*, **12**, 154–164.

Davidson E, Richardson D, Savage KE, Hollinger DY (2006b) A distinct seasonal pattern of the ratio of soil respiration to total ecosystem respiration in a spruce-dominated forest. *Global Change Biology*, **12**, 230–239.

Del Grosso SJ, Parton WJ, Mosier AR, Holland EA, Pendall E, Schimel DS, Ojima DS (2005) Modeling soil CO_2 emissions from ecosystems. *Biogeochemistry*, **73**, 71–91.

Denman KL, Brasseur G, Chidthaisong A *et al.* (2007) Couplings Between Changes in the Climate System and Biogeochemistry. In: *Climate Change 2007: The Physical Science Basis. Contribution of Working Group 1 to the Fourth Assessment Report of the Intergovernmental Panel on Climate Change* (eds Solomon S, Qin D, Manning M, Chen Z, Marquis M, Averyt KB, Tignor M, Miller HL), pp. 499–587. Cambridge, United Kingdom and New York, NY, USA, Cambridge University Press.

Dorrepaal E, Toet S, van Logtestijn RSP, Swart E, van de Weg MJ, Callaghan TV, Aerts R (2009) Carbon respiration from subsurface peat accelerated by climate warming in the subarctic. *Nature*, **460**, 616–619.

Fader M, Rost S, Müller C, Bondeau A, Gerten D (2010) Virtual water content of temperate cereals and maize: Present and potential future patterns. *Journal of Hydrology*, **384**, 218–231.

Falge E, Baldocchi D, Tenhunen J *et al.* (2002) Seasonality of ecosystem respiration and gross primary production as derived from FLUXNET measurements. *Agricultural and Forest Meteorology*, **113**, 53–74.

Fang C, Moncrieff J (2001) The dependence of soil CO_2 efflux on temperature. *Soil Biology and Biochemistry*, **33**, 155–165.

Friedl M, McIver D, Hodges JC *et al.* (2002) Global land cover mapping from MODIS: algorithms and early results. *Remote Sensing of Environment*, **83**, 287–302.

Friedlingstein P, Cox P, Betts R *et al.* (2006) Climate-carbon cycle feedback analysis: results from the C4MIP model intercomparison. *Journal of Climate*, **19**, 3337–3353.

Gerten D, Schaphoff S, Haberlandt U, Lucht W, Sitch S (2004) Terrestrial vegetation and water balance—hydrological evaluation of a dynamic global vegetation model. *Journal of Hydrology*, **286**, 249–270.

Gilmanov T, Tieszen L, Wylie B *et al.* (2005) Integration of CO_2 flux and remotely-sensed data for primary production and ecosystem respiration analyses in the Northern Great Plains: potential for quantitative spatial extrapolation. *Global Ecology and Biogeography*, **27**, 1–292.

Global Soil Data Task (2000) *Global Gridded Surfaces of Selected Soil Characteristics (IGBP-DIS).* Data set available on-line [http://www.daac.ornl.gov] from Oak Ridge National Laboratory Distributed Active Archive Center, Oak Ridge, Tennessee, U.S.A. (Accessed 10 August 2011).

Graf A, Weihermüller L, Huisman JA, Herbst M, Vereecken H (2011) Comment on "Global convergence in the temperature sensitivity of respiration at ecosystem level". *Science*, **331**, 1265; author reply 1265.

Gu Y, Brown JF, Verdin JP, Wardlow B (2007) A five-year analysis of MODIS NDVI and NDWI for grassland drought assessment over the central Great Plains of the United States. *Geophysical Research Letters*, **34**, L06407.

Gu L, Hanson PJ, Mac Post W, Liu Q (2008) A novel approach for identifying the true temperature sensitivity from soil respiration measurements. *Global Biogeochemical Cycles*, **22**, GB4009.

Hanson P, Amthor J (2004) Oak forest carbon and water simulations: model intercomparisons and evaluations against independent data. *Ecological*, **74**, 443–489.

Hashimoto H, Dungan J, White M, Yang F, Michaelis A, Running S, Nemani R (2008) Satellite-based estimation of surface vapor pressure deficits using MODIS land surface temperature data. *Remote Sensing of Environment*, **112**, 142–155.

Heimann M, Reichstein M (2008) Terrestrial ecosystem carbon dynamics and climate feedbacks. *Nature*, **451**, 289–292.

Heinsch F, Zhao M (2006) Evaluation of remote sensing based terrestrial productivity from MODIS using regional tower eddy flux network observations. *IEEE Transactions on Geoscience and Remote Sensing*, **44**, 1908–1925.

Hibbard KA, Law BE, Reichstein M, Sulzman J (2005) An analysis of soil respiration across northern hemisphere temperate ecosystems. *Biogeochemistry*, **73**, 29–70.

Huang N, Niu Z (2013) Estimating soil respiration using spectral vegetation indices and abiotic factors in irrigated and rainfed agroecosystems. *Plant and Soil*, **367**, 535–550.

Janssens I, Lankreijer H, Matteucci G *et al.* (2001) Productivity overshadows temperature in determining soil and ecosystem respiration across European forests. *Global Change Biology*, **7**, 269–278.

Jones C, Cox P, Huntingford C (2003) Uncertainty in climate-carbon-cycle projections associated with the sensitivity of soil respiration to temperature. *Tellus B*, **55B**, 642–648.

Jung M, Reichstein M, Bondeau A (2009) Towards global empirical upscaling of FLUXNET eddy covariance observations: validation of a model tree ensemble approach using a biosphere model. *Biogeosciences*, **6**, 2001–2013.

Jung M, Reichstein M, Margolis HA *et al.* (2011) Global patterns of land-atmosphere fluxes of carbon dioxide, latent heat, and sensible heat derived from eddy covariance, satellite, and meteorological observations. *Journal of Geophysical Research*, **116**, G00J07.

Kimball JS, Jones LA, Member S *et al.* (2009) A Satellite Approach to Estimate Land-Atmosphere CO2 Exchange for Boreal and Arctic Biomes Using MODIS and AMSR-E. *Transactions on Geoscience and Remote Sensing*, **47**, 569–587.

Kirschbaum MUF (1995) The temperature dependence of soil organic matter decomposition, and the effect of global warming on soil organic C storage. *Soil Biology and Biochemistry*, **27**, 753–760.

Kirschbaum MUF (2006) The temperature dependence of organic-matter decomposition—still a topic of debate. *Soil Biology and Biochemistry*, **38**, 2510–2518.

Kirschbaum MUF (2010) The temperature dependence of organic matter decomposition: seasonal temperature variations turn a sharp short-term temperature response into a more moderate annually averaged response. *Global Change Biology*, **16**, 2117–2129.

Krinner G (2005) A dynamic global vegetation model for studies of the coupled atmosphere-biosphere system. *Global Biogeochemical Cycles*, **19**, GB1015.

Kucharik CJ, Barford CC, El Maayar M, Wofsy SC, Monson RK, Baldocchi DD (2006) A multiyear evaluation of a Dynamic Global Vegetation Model at three AmeriFlux forest sites: vegetation structure, phenology, soil temperature, and CO_2 and H_2O vapor exchange. *Ecological Modelling*, **196**, 1–31.

Kuzyakov Y, Gavrichkova O (2010) REVIEW: time lag between photosynthesis and carbon dioxide efflux from soil: a review of mechanisms and controls. *Global Change Biology*, **16**, 3386–3406.

Lasslop G, Reichstein M, Kattge J, Papale D (2008) Influences of observation errors in eddy flux data on inverse model parameter estimation. *Biogeosciences Discussions*, **5**, 751–785.

Lasslop G, Reichstein M, Papale D *et al.* (2010) Separation of net ecosystem exchange into assimilation and respiration using a light response curve approach: critical issues and global evaluation. *Global Change Biology*, **16**, 187–208.

Le Quéré C, Raupach MR, Canadell JG *et al.* (2009) Trends in the sources and sinks of carbon dioxide. *Nature Geoscience*, **2**, 831–836.

Lindroth A, Lagergren F, Aurela M *et al.* (2008) Leaf area index is the principal scaling parameter for both gross photosynthesis and ecosystem respiration of Northern deciduous and coniferous forests. *Tellus B*, **60**, 129–142.

Lloyd J, Taylor J (1994) On the temperature dependence of soil respiration. *Functional ecology*, **8**, 315–323.

Loranty MM, Goetz SJ, Rastetter EB, Rocha AV, Shaver GR, Humphreys ER, Lafleur PM (2010) Scaling an Instantaneous Model of Tundra NEE to the Arctic Landscape. *Ecosystems*, **14**, 76–93.

Mahadevan P, Wofsy SC, Matross DM *et al.* (2008) A satellite-based biosphere parameterization for net ecosystem CO 2 exchange: vegetation Photosynthesis and Respiration Model (VPRM). *Global Biogeochemical Cycles*, **22**, GB2005.

Mahecha MD, Reichstein M, Carvalhais N *et al.* (2010) Global convergence in the temperature sensitivity of respiration at ecosystem level. *Science*, **329**, 838–840.

Massman WJ, Lee X (2002) Eddy covariance flux corrections and uncertainties in long-term studies of carbon and energy exchanges. *Agricultural and Forest Meteorology*, **113**, 121–144.

Migliavacca M, Reichstein M, Richardson AD *et al.* (2011) Semiempirical modeling of abiotic and biotic factors controlling ecosystem respiration across eddy covariance sites. *Global Change Biology*, **17**, 390–409.

Mitchell TD, Jones PD (2005) An improved method of constructing a database of monthly climate observations and associated high-resolution grids. *International Journal of Climatology*, **25**, 693–712.

Oesterle H, Gerstengarbe F, Werner PC (2003) Homogenisierung und Aktualisierung des Klimadatensatzes der Climate Research Unit der University of East Anglia, Norwich. *Terra Nostra*, **6**, 326–329.

Olofsson P, Lagergren F, Lindroth A, Lindström J, Klemedtsson L, Kutsch W, Eklundh L (2008) Towards operational remote sensing of forest carbon balance across Northern Europe. *Biogeosciences*, **5**, 817–832.

ORNL (2011) *Oak Ridge National Laboratory Distributed Active Archive Center (ORNL DAAC), FLUXNET Web Page.* Available online [http://fluxnet.ornl.gov] from ORNL DAAC, Oak Ridge, Tennessee, U.S.A. (Accessed 5 January 2011).

ORNL (2010) *Oak Ridge National Laboratory Distributed Active Archive Center (ORNL DAAC), World Map of the Koppen-Geiger Climate Classification.* Available online [http://webmap.ornl.gov/wcsdown/dataset.jsp?ds_id=10012] from ORNL DAAC, Oak Ridge, Tennessee, U.S.A. (Accessed 10 February 2011).

Pan Y, Birdsey RA, Fang J *et al.* (2011) A large and persistent carbon sink in the world's forests. *Science*, **333**, 988–993.

Papale D (2006) Towards a standardized processing of Net Ecosystem Exchange measured with eddy covariance technique: algorithms and uncertainty estimation. *Biogeosciences*, **3**, 571–583.

Papale D, Valentini R (2003) A new assessment of European forests carbon exchanges by eddy fluxes and artificial neural network spatialization. *Global Change Biology*, **9**, 525–535.

Peel M, Finlayson B, McMahon T (2007) Updated world map of the Köppen-Geiger climate classification. *Hydrology and Earth System Sciences Discussions*, **4**, 439–473.

Pereira JS, Mateus JA, Aires LM *et al*. (2007) Net ecosystem carbon exchange in three contrasting Mediterranean ecosystems – the effect of drought. *Biogeosciences*, **4**, 791–802.

Rahman AF, Sims DA, Cordova VD, El-Masri BZ (2005) Potential of MODIS EVI and surface temperature for directly estimating per-pixel ecosystem C fluxes. *Geophysical Research Letters*, **32**, L19404.

Raich JW, Schlesinger WH (1992) The global carbon dioxide flux in soil respiration and its relationship to vegetation and climate. *Tellus B*, **44**, 81–99.

Raich J, Tufekciogul A (2000) Vegetation and soil respiration: correlations and controls. *Biogeochemistry*, **48**, 71–90.

Rebmann C, Zeri M, Lasslop G, Mund M, Kolle O, Schulze E-D, Feigenwinter C (2010) Treatment and assessment of the CO2-exchange at a complex forest site in Thuringia, Germany. *Agricultural and Forest Meteorology*, **150**, 684–691.

Reich PB (2010) The carbon dioxide exchange. *Science*, **329**, 774–775.

Reichstein M, Beer C (2008) Soil respiration across scales: the importance of a model–data integration framework for data interpretation. *Journal of Plant Nutrition and Soil Science*, **171**, 344–354.

Reichstein M, Falge E, Baldocchi D *et al*. (2005) On the separation of net ecosystem exchange into assimilation and ecosystem respiration: review and improved algorithm. *Global Change Biology*, **11**, 1424–1439.

Reichstein M, Ciais P, Papale D *et al*. (2007) Reduction of ecosystem productivity and respiration during the European summer 2003 climate anomaly: a joint flux tower, remote sensing and modelling analysis. *Global Change Biology*, **13**, 634–651.

Richardson AD, Braswell BH, Hollinger DY *et al*. (2006a) Comparing simple respiration models for eddy flux and dynamic chamber data. *Agricultural and Forest Meteorology*, **141**, 219–234.

Richardson AD, Hollinger DY, Burba GG *et al*. (2006b) A multi-site analysis of random error in tower-based measurements of carbon and energy fluxes. *Agricultural and Forest Meteorology*, **136**, 1–18.

Richardson AD, Mahecha MD, Falge E *et al*. (2008) Statistical properties of random CO2 flux measurement uncertainty inferred from model residuals. *Agricultural and Forest Meteorology*, **148**, 38–50.

Rudolf B, Becker A, Chneider U, Meyer-Christoffer A, Ziese M (2010) *The new 'GPCC full data reanalysis version 5' providing high-quality gridded monthly precipitation data for the global land-surface is public available since December 2010*, GPCC Status Report.

Running S, Nemani R, Heinsch F, Zhao M, Reeves M, Hashimoto H (2004) A continuous satellite-derived measure of global terrestrial primary production. *BioScience*, **54**, 547–560.

Ryan MG (1991) Effects of climate change on plant respiration. *Ecological Applications*, **1**, 157–167.

Ryan MG, Law BE (2005) Interpreting, measuring, and modeling soil respiration. *Biogeochemistry*, **73**, 3–27.

Saatchi SS, Harris NL, Brown S *et al*. (2011) Benchmark map of forest carbon stocks in tropical regions across three continents. *Proceedings of the National Academy of Sciences of the United States of America*, **108**, 9899–9904.

Sabine CL, Heimann M, Artaxo P (2004) Current Status and Past Trends of Global Carbon Cycle. In: *The Global Carbon Cycle: Integrating Humans, Climate and the Natural World* (eds Field CB, Raupach MR), pp. 17–44. Washington, Island Press.

Salomonson VV, Appel I (2004) Estimating fractional snow cover from MODIS using the normalized difference snow index. *Remote Sensing of Environment*, **89**, 351–360.

Samanta A, Ganguly S, Vermote E, Nemani RR, Myneni RB (2012) Why Is Remote Sensing of Amazon Forest Greenness So Challenging? *Earth Interactions*, **16**, 1–14.

Schaphoff S, Heyder U, Ostberg S, Gerten D, Heinke J, Lucht W (2013) Contribution of permafrost soils to the global carbon budget. *Environmental Research Letters*, **8**, 014026.

Schimel D, House J, Hibbard K *et al*. (2001) Recent patterns and mechanisms of carbon exchange by terrestrial ecosystems. *Nature*, **414**, 169–172.

Schindlbacher A, Zechmeister-Boltenstern S, Jandl R (2009) Carbon losses due to soil warming: do autotrophic and heterotrophic soil respiration respond equally? *Global Change Biology*, **15**, 901–913.

Schmugge T (1978) Remote sensing of surface soil moisture. *Journal of Applied Meteorology*, **17**, 1549–1557.

Schnur MT, Xie H, Wang X (2010) Estimating root zone soil moisture at distant sites using MODIS NDVI and EVI in a semi-arid region of southwestern USA. *Ecological Informatics*, **5**, 400–409.

Schubert P, Eklundh L, Lund M, Nilsson M (2010) Estimating northern peatland CO_2 exchange from MODIS time series data. *Remote Sensing of Environment*, **114**, 1178–1189.

Sims D, Rahman A, Cordova V *et al*. (2008) A new model of gross primary productivity for North American ecosystems based solely on the enhanced vegetation index and land surface temperature from MODIS. *Remote Sensing of Environment*, **112**, 1633–1646.

Sitch S, Smith B, Prentice IC *et al*. (2003) Evaluation of ecosystem dynamics, plant geography and terrestrial carbon cycling in the LPJ dynamic global vegetation model. *Global Change Biology*, **9**, 161–185.

Tjoelker MG, Oleksyn J, Reich PB (2001) Modelling respiration of vegetation: evidence for a general temperature-dependent Q10. *Global Change Biology*, **7**, 223–230.

Verstraeten WW, Veroustraete F, van der Sande CJ, Grootaers I, Feyen J (2006) Soil moisture retrieval using thermal inertia, determined with visible and thermal spaceborne data, validated for European forests. *Remote Sensing of Environment*, **101**, 299–314.

Vourlitis GL, Verfaillie J, Oechel WC, Hope A, Stow D, Engstrom R (2003) Spatial variation in regional CO_2 exchange for the Kuparuk River Basin, Alaska over the summer growing season. *Global Change Biology*, **9**, 930–941.

Wan Z (2008) New refinements and validation of the MODIS Land-Surface Temperature/Emissivity products. *Remote Sensing of Environment*, **112**, 59–74.

Wan Z, Dozier J (1996) A generalized split-window algorithm for retrieving land-surface temperature from space. *IEEE Transactions on Geoscience and Remote Sensing*, **34**, 892–905.

Wan Z, Li Z (2008) Radiance-based validation of the V5 MODIS land-surface temperature product. *International Journal of Remote Sensing*, **29**, 5373–5395.

Wang L, Qu JJ (2009) Satellite remote sensing applications for surface soil moisture monitoring: a review. *Frontiers of Earth Science in China*, **3**, 237–247.

Williams M, Richardson AD, Reichstein M *et al*. (2009) Improving land surface models with FLUXNET data. *Biogeosciences*, **6**, 1341–1359.

Xiao J, Zhuang Q, Law BE *et al*. (2011) Assessing net ecosystem carbon exchange of U.S. terrestrial ecosystems by integrating eddy covariance flux measurements and satellite observations. *Agricultural and Forest Meteorology*, **151**, 60–69.

Xiao J, Chen J, Davis KJ, Reichstein M (2012) Advances in upscaling of eddy covariance measurements of carbon and water fluxes. *Journal of Geophysical Research*, **117**, G00J01.

Xu L, Baldocchi DD (2004) Seasonal variation in carbon dioxide exchange over a Mediterranean annual grassland in California. *Agricultural and Forest Meteorology*, **123**, 79–96.

Yamaji T, Sakai T, Endo T *et al*. (2007) Scaling-up technique for net ecosystem productivity of deciduous broadleaved forests in Japan using MODIS data. *Ecological Research*, **23**, 765–775.

Yang F, Ichii K, White MA *et al*. (2007) Developing a continental-scale measure of gross primary production by combining MODIS and AmeriFlux data through Support Vector Machine approach. *Remote Sensing of Environment*, **110**, 109–122.

Yuan W, Luo Y, Li X *et al*. (2011) Redefinition and global estimation of basal ecosystem respiration rate. *Global Biogeochemical Cycles*, **25**, GB4002.

Yvon-Durocher G, Caffrey JM, Cescatti A *et al*. (2012) Reconciling the temperature dependence of respiration across timescales and ecosystem types. *Nature*, **487**, 472–476.

Zaehle S, Sitch S, Smith B, Hatterman F (2005) Effects of parameter uncertainties on the modeling of terrestrial biosphere dynamics. *Global Biogeochemical Cycles*, **19**, GB3020.

Zhou T, Shi P, Hui D, Luo Y (2009) Global pattern of temperature sensitivity of soil heterotrophic respiration (Q 10) and its implications for carbon-climate feedback. *Journal of Geophysical Research*, **114**, G02016.

Supporting Information

Additional Supporting Information may be found in the online version of this article:

Table S1 Investigated Fluxnet sites with *in situ* climate and land cover classification.
Table S2 Number of Fluxnet sites per IGBP land cover class from *in situ* and MODIS product, respectively.
Table S3 Re_{ref} parameter table for each fitted biome, parameters p1–p3 refer to Eqn 6. 'lwr' and 'upr' indicate lower and upper confidence intervals (2.5% and 97.5%), respectively.
Table S4 Re_{std} parameter table for each aggregated biome, parameters p1–p5 refer to Eqn 7, 8, 9. 'lwr' and 'upr' indicate lower and upper confidence intervals (2.5% and 97.5%), respectively.
Table S5 Evaluation of temperature functions for the Re_{std} response. Each biome is fitted individually (not WL) and R2 and AIC (Akaike's Information Criterion) are mean values over all fits. DF, Degrees of freedom.
Table S6 Re evaluation for each fitted biome, based on fivefold cross-validation.
Figure S1. MODIS NDSI vs. MODIS Snow index for Temperature-Limited sites, Scatter-plots of EVI against nighttime LST (a) and (b), against ecosystem respiration (c) and against Doy of Year (d).
Figure S2. Correlations between Terra and Aqua LST products for nighttime LST (a) and daytime LST (c) and for linearly adjusted Aqua LST products (b, d).
Figure S3. Definition of the dry season in the water-limited (WL) biome.